J. Fluid Mech. (1980), *vol.* 99, *part* 1, *pp.* 185–224
Printed in Great Britain

A three-dimensional boundary-layer separation

By F. T. SMITH†

Applied Mathematics Department, University of Western Ontario,
London, Ontario, Canada

(Received 7 March 1979 and in revised form 15 August 1979)

A nonlinear three-dimensional boundary-layer problem governing the flow upstream of a particular disturbance (e.g. a shallow obstacle) at the wall is considered. The upstream response, a free interaction, takes place under zero displacement of the boundary layer, and the solution is found numerically using Fourier series truncation and varying the number of terms kept in the series. In one part of the flow field regular separation is encountered, beyond which the motion becomes strongly attached to the wall elsewhere in the flow field. Analytically, local structural investigations then suggest that the attached part of the upstream response terminates at a line singularity, while the separated part can continue indefinitely far downstream. The former structure leads to a new set of similarity solutions of the three-dimensional boundary-layer equations, while the latter develops a vortex sheet formation. The three-dimensional flow problem has most relevance to pipe flows, but some connexion also with external flows, and the implications for these are discussed.

1. Introduction

Detailed understanding of separation in two-dimensional laminar flows at high Reynolds numbers has advanced considerably following the breakthrough by Stewartson & Williams (1969) in their study of supersonic separation. In external flow situations progress has been made with the separation phenomenon not only in supersonic boundary layers (reviewed by Stewartson 1974) but also in incompressible-fluid or subsonic boundary layers (Sychev 1972; Messiter 1975; Smith 1977*a*, 1979*a*) and in jet flows (Smith & Duck 1977). Messiter (1979) has recently reviewed this progress. In internal flows also, a similar degree of progress has proved possible with two-dimensional or axisymmetric motions (Smith 1976*a*, 1977*b*, 1979*b*).

Detailed understanding of three-dimensional separation, on the other hand, has been severely limited because of the obviously much more complicated nature of the mechanisms involved. The three-dimensional situation is clearly the more important physically but, although in external flow separation from a three-dimensional body is believed to be generally of a quasi-two-dimensional form locally (J. H. B. Smith 1977; Smith 1978*a*), no satisfactory account of a genuinely three-dimensional separation has been advanced yet, in external or internal motions, except for the works of Sykes (1979) and Professor O. R. Burggraf & Dr P. W. Duck (1978–1979 private communications). The latter concentrate on supersonic, triple-deck (cf. Smith, Sykes & Brighton 1977) flow past a particular three-dimensional ramp, and the former solves numerically

† Permanent address: Mathematics Department, Imperial College, London, S.W. 7, U.K.

0022-1120/80/4480-1420 $02.00

a three-dimensional pipe-flow problem (of Smith 1976*b*) which involves zero displacement of the boundary layer (as described below).

Our concern is also with the Smith (1976*b*) pipe-flow problem (see also comments at the end of § 1) but our standpoint and aims are rather different from those of Sykes' (1979) complementary study. He investigates the effects of particular three-dimensional obstacles, of length (streamwise) $O(a^*)$ and height (normally) $O(a^*R^{-\frac{1}{3}}h)$, in a boundary layer, where a^* is the radius of the pipe, $R(\gg 1)$ is the Reynolds number (see below) and h is an $O(1)$ parameter ($0 \leqslant h < \infty$). For such obstacles upstream influence is generated on an $O(a^*)$ length scale according to Smith (1976*b*) (who considered solutions for $h \ll 1$), and Sykes (1979) obtains solutions effectively for a number of values of h. Our interest, however, centres on the upper limit of the problem of Smith (1976*b*) and Sykes (1979), in the sense that h is supposed to be large (but not so large that the asymptotic structure of Smith 1976*b* is disturbed: strictly, $1 \ll h \ll R^q$ for all $q > 0$). In that case the upstream response can be expected to be pushed as far upstream as possible and, after a nonlinear development, the upstream response must terminate (at the onset of the obstacle) with relatively large velocities and pressures in order to be able to negotiate the relatively large obstacle. Similar arguments have been applied in two-dimensional flows by Stewartson & Williams (1969, 1973), Smith & Stewartson (1973*a*, *b*), Smith (1977*a*). The major question then is: how does the upstream response terminate?

The answer to the question above should in particular enable a description of the flow past obstacles much steeper than those (of slope $R^{-\frac{1}{3}}$) above to be put forward and so allow inroads to be made into the more realistic problems of flow past more severe three-dimensional obstacles. However, the question does necessitate a numerical study of the entire three-dimensional free interaction stemming from Smith's (1976*b*) linearized treatment, followed by an analysis of the terminal structure of the upstream response, and that, essentially, is the aim of the present work. Fortunately the entire upstream response can be obtained by integrating the free interaction forward (at least, until separation is encountered: see §§ 2 and 3 below) without change of boundary conditions. Nevertheless, severe numerical difficulties do arise in treating the three-dimensional boundary-layer problem in a satisfactory manner, as Sykes (1979) points out. Our treatment, involving Fourier series truncation and a gradual increasing of the number of terms kept in the series, is described in § 2 and 3. The solutions for the upstream boundary layer are also presented in § 3. They show three-dimensional separation (which is encountered here in a regular fashion; cf. Goldstein 1948) setting in at one part of the flow field, followed by a strong attachment phenomenon at another part of the flowfield. Then § 4 considers the ultimate form of the upstream response. It is predicted that the attached part terminates along a line singularity and the terminal form there leads to a new set of similarity solutions of the three-dimensional boundary-layer equations (§ 4.1). In contrast, the separated part can extend infinitely far downstream in principle and it acquires a vortex-sheet formation there (§ 4.2). The analysis of §§ 4.1, 4.2 is compared with the full numerical solutions of § 3 in § 4.3. Finally, § 5 provides some interpretation and discussion of the results and analysis.

The three-dimensional boundary-layer problem tackled below is of most relevance in pipe flows (Smith 1976*b*) then, in which context we introduce the flow variables. The cylindrical polar co-ordinates (x, r, θ), corresponding velocities (u, v, w) and the pressure p are used, where the lengths, velocities and pressure have

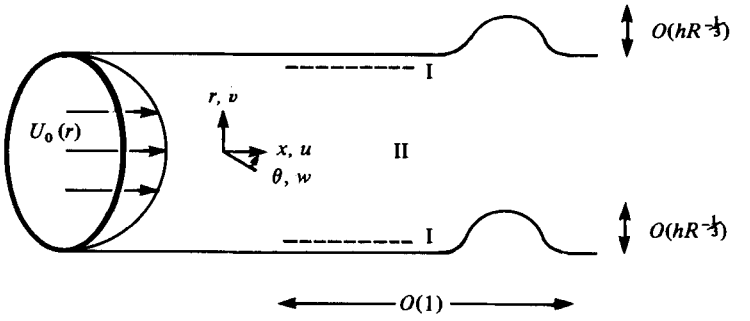

FIGURE 1. The geometry and the co-ordinates for the upstream response of the three-dimensional pipe flow studied in this paper, assuming an obstacle of slope $\gg R^{-\frac{1}{3}}$ downstream.

been non-dimensionalized with respect to a^*, U_∞^* and ρU_∞^{*2} respectively, U_∞^* is a characteristic speed of the pipe flow far upstream and ρ is the fluid density (see figure 1). The flow far upstream is taken to be Poiseuille flow, although it should be possible later to treat more general oncoming forms also. The Reynolds number is $R = U_\infty^* a^* \nu^{-1} \gg 1$, where ν is the kinematic viscosity of the fluid, and the fluid is assumed to be incompressible and its motion to be laminar and steady. The upstream response then occurs with x, θ of $O(1)$ $(0 \leqslant \theta < 2\pi)$ (figure 1) and the oncoming Poiseuille motion holding for $x \to -\infty$ is taken to have the form

$$u = \tfrac{1}{2}(1-r^2), \quad v = w = 0, \quad p \sim -2x/R. \tag{1.1}$$

However, since only the boundary layer induced (with zero displacement) near the pipe wall needs to be examined here, the problem of this paper also has some connexions with certain external flow situations, as Sykes (1979) notes. For example, the triple-deck external flow problem of Smith *et al.* (1977) reduces to our one with zero displacement if the length scales of their obstacles are reduced significantly (in much the same manner as that described by Smith 1973 in planar motions). Only the periodicity of our flow problem with respect to θ tends to limit its applicability to many external situations, therefore.

2. The flow structure, governing equations and numerical scheme

The flow structure is set up predominantly in the boundary layer (I) of thickness $O(R^{-\frac{1}{3}})$. In I,

$$(u, v, w, p) = [R^{-\frac{1}{3}}U(x, Y, \theta), -R^{-\frac{2}{3}}V(x, Y, \theta), R^{-\frac{1}{3}}W(x, Y, \theta), R^{-\frac{2}{3}}P(x, \theta)] \tag{2.1}$$

to leading order and $r = 1 - R^{-\frac{1}{3}}Y$, where Y is $O(1)$. The governing equations are therefore those expressing continuity, x momentum and θ momentum:

$$\frac{\partial U}{\partial x} + \frac{\partial V}{\partial Y} + \frac{\partial W}{\partial \theta} = 0, \tag{2.2a}$$

$$U\frac{\partial U}{\partial x} + V\frac{\partial U}{\partial Y} + W\frac{\partial U}{\partial \theta} = -\frac{\partial P}{\partial x} + \frac{\partial^2 U}{\partial Y^2}, \tag{2.2b}$$

$$U\frac{\partial W}{\partial x} + V\frac{\partial W}{\partial Y} + W\frac{\partial W}{\partial \theta} = -\frac{\partial P}{\partial \theta} + \frac{\partial^2 W}{\partial Y^2}, \tag{2.2c}$$

while the r-momentum equation is satisfied to leading order since $\partial P/\partial Y = 0$. The boundary conditions on (2.2a–c) are

$$U = V = W = 0 \quad \text{at} \quad Y = 0, \tag{2.3a}$$

$$U \to Y, \quad V \to 0, \quad W \to 0, \quad P \to 0 \quad \text{as} \quad x \to -\infty, \tag{2.3b}$$

$$U \sim Y + o(1) \quad \text{as} \quad Y \to \infty, \tag{2.3c}$$

$$\text{periodicity in } \theta. \tag{2.3d}$$

Here (2.3a) is the no-slip condition, (2.3b) matches the flow to the Poiseuille shear far upstream, and (2.3c) is a zero displacement condition necessary to match I with the flow in the core (II, wherein $0 \leqslant r < 1$). For, if the displacement from the boundary layer were non-zero ($U - Y \nrightarrow 0$ as $Y \to \infty$), then in the core the pressure would have to be $O(R^{-\frac{1}{4}})$ and would satisfy a linear equation with homogeneous boundary conditions. We propose (as in Smith 1976b) that in general there is no non-trivial solution for such a core pressure, which proposition leads us to the constraint (2.3c). In fact, in II the perturbations of (1.1) are only $O(R^{-\frac{3}{8}})$ and the solution has the form

$$(u, v, w, p) = (\tfrac{1}{2}(1-r^2), 0, 0, 0) + R^{-\frac{3}{8}}(u_1, v_1, w_1, p_1). \tag{2.4a}$$

Here u_1, v_1, w_1, p_1 satisfy the linearized inviscid equations of motion and the boundary conditions

$$p_1 \to P(x, \theta), \quad u_1 \sim O((1-r)^{-1}), \quad v_1 \sim O(1), \quad w_1 \sim O((1-r)^{-1}) \tag{2.4b}$$

as $r \to 1-$, to merge with (2.1). The core flow therefore has but a passive role in the flow structure and can be determined only after the boundary-layer flow in I has been found. The existence of solutions for u_1, v_1, w_1, p_1 satisfying (2.4b) is discussed by Smith (1976b). Finally, the condition (2.3d) of periodicity will be made specific below.

The problem (2.2a–c) to (2.3a–d) is a closed and parabolic one (at least, until any flow reversal is encountered: see § 3 below), and is the main concern of this paper. The boundary layer starts its deviation from the incoming Poiseuille form ($U = Y$, $V = W = P = 0$) far upstream, for $x \to -\infty$, where

$$\left.\begin{aligned} U &= Y - b_1 \mathscr{L}(Y)\, e^x \cos(\theta - \theta_0) + O(e^{2x}), \\ V &= O(e^{2x}), \\ P &= b_1 e^x \cos(\theta - \theta_0) + O(e^{2x}), \\ W &= b_1 \mathscr{L}(Y)\, e^x \sin(\theta - \theta_0) + O(e^{2x}) \end{aligned}\right\} \tag{2.5}$$

(Smith 1976b), θ_0 is an arbitrary constant and $\mathscr{L}(Y)$ satisfies

$$\mathscr{L}'' - Y\mathscr{L} = -1, \quad \mathscr{L}(0) = \mathscr{L}(\infty) = 0.$$

The constant b_1 in (2.5) is unknown: it is determined, along with all the arbitrary constants b_n which arise in the successive $O(e^{nx})$ terms implied in (2.5), by the particular downstream mechanism provoking the boundary-layer flow (as in the three-dimensional work of Sykes (1979) and Smith (1976b); cf. the two-dimensional triple-deck studies of Stewartson (1970), Smith & Stewartson (1973a, b), Smith (1974), Rizzetta, Burggraf & Jenson (1978), where only one arbitrary constant arises). Here we consider the inverse problem in which the constants $b_1, b_2, \ldots$ are specified and the solution to (2.2a–c), (2.3a–d) is allowed to develop, nonlinearly, from its initial deviation (2.5).

The necessarily numerical investigation of this development will now be described; discussion of its physical significance is deferred until § 5.

First we observe that, from the properties of (2.2*a–c*) for $Y \gg 1$, (2.3*c*) implies the algebraic behaviour

$$\left.\begin{aligned} U &\sim Y + C(x,\theta)\, Y^{-1} + O(Y^{-2}), \\ V &\sim E(x,\theta) + F(x,\theta)\, Y^{-1} + O(Y^{-2}), \\ W &\sim D(x,\theta)\, Y^{-1} + O(Y^{-2}), \end{aligned}\right\} \quad \text{when} \quad Y \gg 1, \tag{2.6a}$$

where

$$\frac{\partial C}{\partial x} = -\frac{\partial D}{\partial \theta}, \quad \frac{\partial D}{\partial x} = \frac{-\partial P}{\partial \theta}, \quad E = \frac{-\partial P}{\partial x} - \frac{\partial C}{\partial x} \tag{2.6b}$$

and the functions $C(x,\theta)$, $D(x,\theta)$, $E(x,\theta)$, $F(x,\theta)$ are to be determined. Next, we make the periodicity condition (2.3*d*) specific by concentrating on a motion which is symmetric about the plane $\theta = 0, \pi$ (figure 1). Although some loss of generality is involved, this symmetry enables the numerical task to be made lighter while preserving the essential three-dimensional (non-axisymmetric) nature of the problem. Thus (2.3*d*) becomes

$$W = 0 \quad \text{at} \quad \theta = 0, \pi \tag{2.7}$$

and $\theta_0 = 0$ in (2.5). The two conditions in (2.7) can be applied, despite the single θ-derivatives in (2.2*a–c*), because of the unknown streamwise growth rate of the solution.

Initially we tried complete central differencing of the problem (2.2*a–c*), (2.3*a, b*), (2.6*a, b*), (2.7), that being perhaps the most direct and usually reliable method of numerical solution. However, it was found that such a treatment could not cope adequately enough with the three-dimensional variation of the motion, especially the θ-variation. Therefore we turned to a series truncation technique, an extension of those successfully employed by Dennis & Chang (1970), among others, in two-dimensional numerical work. A solution to (2.2*a–c*), (2.3*a, b*), (2.6*a, b*) and (2.7) is sought in the Fourier series form

$$(U, V, W, P) = \sum_{n=-\infty}^{\infty} e^{in\theta}\,[f_n(x, Y), g_n(x, Y), -ih_n(x, Y), p_n(x)] \quad (f_n, g_n, h_n, p_n \text{ real}), \tag{2.8a}$$

where, from (2.7),

$$f_{-n} \equiv f_n, \quad g_{-n} \equiv g_n, \quad h_{-n} \equiv -h_n, \quad p_{-n} \equiv p_n \tag{2.8b}$$

if $n > 0$, and $h_0 \equiv 0$; thus the θ dependence and the conditions (2.7) are dealt with by the trigonometric functions implied in (2.8*a, b*). Substitution of (2.8*a, b*) into the governing equations (2.2*a–c*) and equating coefficients of equal powers of $e^{i\theta}$ leads to an infinite-ordered set of coupled partial differential equations in x, Y only. For computational purposes the infinite set was then truncated (at M, say) by considering only the first $(4M+3)$ distinct equations of the set, for f_j, g_j, h_j, p_j with $0 \leqslant j \leqslant M$ but $h_0 \equiv 0$. The truncated set of equations for $1 \leqslant n \leqslant M$ is:

$$\frac{\partial f_0}{\partial x} + \frac{\partial g_0}{\partial Y} = 0, \tag{2.9a}$$

$$\frac{\partial^2 f_0}{\partial Y^2} - \frac{dp_0}{dx} - f_0 \frac{\partial f_0}{\partial x} - g_0 \frac{\partial f_0}{\partial Y} = 2 \sum_{j=1}^{M} \left(f_j \frac{\partial f_j}{\partial x} + g_j \frac{\partial f_j}{\partial Y} - j h_j F_j \right); \tag{2.9b}$$

$$\frac{\partial f_n}{\partial x}+\frac{\partial g_n}{\partial Y}+nh_n=0, \tag{2.10a}$$

$$\frac{\partial^2 f_n}{\partial Y^2}-\frac{dp_n}{dx}-f_0\frac{\partial f_n}{\partial x}-f_n\frac{\partial f_0}{\partial x}-g_0\frac{\partial f_n}{\partial Y}-g_n\frac{\partial f_0}{\partial Y}$$
$$=\sum_{j=1}^{M-n}\left[\frac{\partial}{\partial x}(f_jf_{n+j})+g_j\frac{\partial f_{n+j}}{\partial Y}+g_{n+j}\frac{\partial f_j}{\partial Y}-jh_{n+j}f_j-(n+j)h_jf_{n+j}\right]$$
$$+\sum_{j=1}^{n-1}\left[f_j\frac{\partial f_{n-j}}{\partial x}+g_j\frac{\partial f_{n-j}}{\partial Y}+jh_{n-j}f_j\right], \tag{2.10b}$$

$$\frac{\partial^2 h_n}{\partial Y^2}+np_n-f_0\frac{\partial h_n}{\partial x}-g_0\frac{\partial h_n}{\partial Y}=\sum_{j=1}^{M-n}\left[f_j\frac{\partial h_{n+j}}{\partial x}-f_{n+j}\frac{\partial h_j}{\partial x}+g_j\frac{\partial h_{n+j}}{\partial Y}-g_{n+j}\frac{\partial h_j}{\partial Y}\right]$$
$$-n\sum_{j=1}^{M-n}h_jh_{n+j}+\sum_{j=1}^{n-1}\left[f_j\frac{\partial h_{n-j}}{\partial x}+g_j\frac{\partial h_{n-j}}{\partial Y}+jh_jh_{n-j}\right]. \tag{2.10c}$$

Thus the (mean flow) terms f_0, g_0, p_0 are governed by the uncoupled but nonlinear equations (2.9a, b), whereas the remaining terms f_n, g_n, h_n, p_n for $1 \leqslant n \leqslant M$ which dictate the θ variation (from (2.7)) are governed by a coupled but linear set (2.10a–c). The boundary conditions on f_0, g_0, p_0 are

$$\left.\begin{aligned} &f_0 \sim Y+O(Y^{-2}), \quad g_0 \to -dp_0/dx \quad \text{as} \quad Y\to\infty,\\ &f_0=g_0=0 \quad \text{at} \quad Y=0,\\ &f_0\to Y, \quad g_0\to 0, \quad p_0\to 0 \quad \text{as} \quad x\to-\infty, \end{aligned}\right\} \tag{2.11}$$

from (2.3a, b), (2.6a, b). Those on f_n, g_n, h_n, p_n for $1 \leqslant n \leqslant M$ are, similarly,

$$\left.\begin{aligned} &\frac{\partial f_n}{\partial x}+nh_n \sim O(Y^{-2}), \quad \frac{\partial h_n}{\partial x}-\frac{np_n}{Y} \sim O(Y^{-2}) \quad \text{as} \quad Y\to\infty,\\ &f_n=g_n=h_n=0 \quad \text{at} \quad Y=0,\\ &f_n\to 0, \quad g_n\to 0, \quad h_n\to 0, \quad p_n\to 0 \quad \text{as} \quad x\to-\infty. \end{aligned}\right\} \tag{2.12}$$

The numerical procedure adopted for (2.9)–(2.12) was fairly straightforward in principle but involved many cumbersome matrix manipulations and so here we will describe only the basic essentials of the procedure. The equations (2.9)–(2.10) were discretized using two- and three-point central differences and averages (see below), while the outer conditions (for $Y\to\infty$) in (2.11) and (2.12) were generally replaced by corresponding one-point and two-point difference constraints respectively, at a suitably large value (Y_∞) of Y, with the contributions marked $O(Y^{-2})$ being neglected. Thus, with mesh widths of Δx in x, ΔY in Y, at a particular calculation point

$$(x+\tfrac{1}{2}\Delta x, Y_k)$$

for the momentum equations (2.9b), (2.10b, c) the terms dp_n/dx, np_n, $\partial^2 f_n/\partial Y^2$, $f_j\,\partial f_{n-j}/\partial x$, $g_j\,\partial f_{n+j}/\partial Y$, $h_{n+j}f_j$, for example, were replaced by the centred differences or averages

$$\frac{p_n-\bar{p}_n}{\Delta x}, \quad \frac{n(p_n+\bar{p}_n)}{2}, \quad \frac{f_n^{(k+1)}-2f_n^{(k)}+f_n^{(k-1)}+\bar{f}_n^{(k+1)}-2\bar{f}_n^{(k)}+\bar{f}_n^{(k-1)}}{2(\Delta Y)^2},$$

$$\frac{[f_j^{(k)}+\bar{f}_j^{(k)}][f_{n-j}^{(k)}-\bar{f}_{n-j}^{(k)}]}{2\Delta x}, \quad \frac{[g_j^{(k)}+\bar{g}_j^{(k)}][f_{n+j}^{(k+1)}-f_{n+j}^{(k-1)}+\bar{f}_{n+j}^{(k+1)}-\bar{f}_{n+j}^{(k-1)}]}{8\Delta Y},$$

$$\tfrac{1}{4}[h_{n+j}^{(k)}+\bar{h}_{n+j}^{(k)}][f_j^{(k)}+\bar{f}_j^{(k)}],$$

respectively, for $K-1 \geqslant k \geqslant 1$, where $Y_\infty = (K-1)\Delta Y$. Here $\bar{f}_n^{(k)}, f_n^{(k)}$ denote in turn the known and unknown values, at the $(k-1)$th mesh point $Y = Y_k = (k-1)\Delta Y$ from the surface $Y = 0$, of the function f_n at the two successive stations x, $x+\Delta x$, and similarly for the other functions shown. Discretizations analogous to those above were applied to the other terms in the momentum equations (2.9*b*), (2.10*b*, *c*). In the continuity equations (2.9*a*), (2.10*a*) the discretizations were centred on the points $(x+\frac{1}{2}\Delta x, Y_k - \frac{1}{2}\Delta Y)$, in the form

$$\frac{f_n^{(k)} - \bar{f}_n^{(k)} + f_n^{(k-1)} - \bar{f}_n^{(k-1)}}{2\Delta x} + \frac{g_n^{(k)} - g_n^{(k-1)} + \bar{g}_n^{(k)} - \bar{g}_n^{(k-1)}}{2\Delta Y} + \frac{n}{4}(h_n^{(k)} + h_n^{(k-1)} + \bar{h}_n^{(k)} + \bar{h}_n^{(k-1)}) = 0$$

for $K \geqslant k \geqslant 1$ and all $n \geqslant 0$. The outer boundary conditions set were

$$\frac{1}{\Delta Y}[f_0^{(K)} - f_0^{(K-1)}] = 1, \quad \tfrac{1}{2}[g_0^{(K)} + \bar{g}_0^{(K)}] = -\frac{1}{\Delta x}(p_0 - \bar{p}_0)$$

for $n = 0$ (cf. (2.11)), and for $n \geqslant 1$

$$\frac{1}{\Delta x}[f_n^{(K)} - \bar{f}_n^{(K)}] + \frac{n}{2}[h_n^{(K)} + \bar{h}_n^{(K)}] = 0, \quad \frac{1}{\Delta x}[h_n^{(K)} - \bar{h}_n^{(K)}] = \frac{n}{2Y_\infty}[p_n + \bar{p}_n];$$

cf. (2.12). Other versions tested for the outer boundary conditions produced changes in the finite difference solutions well within the accepted limits of accuracy. The wall conditions in (2.11), (2.12) were set in the obvious way. Let the discrete versions of (2.9)–(2.12) be denoted by dashes. Then, given the whole finite difference solution at the station x, the solution at the next step $(x+\Delta x)$ was found by iteration from an initial guess as follows: (i) First, new guesses for all the $f_n^{(k)}$, $g_n^{(k)}$, $h_n^{(k)}$, p_n for $1 \leqslant n \leqslant M$ were derived by solving the linear equations (2.10′). (ii) Next, the terms newly guessed in (i) (or (iii) below) were inserted into the right-hand sides of (2.9′) and the nonlinear equations (2.9′*a*, *b*) were solved by Newton iteration to yield new guesses for $f_0^{(k)}$, $g_0^{(k)}$, p_0. (iii) Then the equations (2.10′) were re-solved for each n in turn, using the latest values for $f_0^{(k)}$, $g_0^{(k)}$, p_0 and $f_j^{(k)}$, $g_j^{(k)}$, $h_j^{(k)}$, p_j with $j \neq n$ in the right-hand sides. The process (ii)–(iii) was continued until all successive iterates differed by less than a prescribed tolerance q. The same tolerance q was set on the Newton iteration involved in each step (ii). To start off the nonlinear development of the boundary layer an initial non-symmetric small kick

$$P_{-\infty} = \sum_{n=-M}^{M} b_n e^{in\theta} \tag{2.13}$$

(consistent with (2.5)) was given to the pressure field at an initial station $x = x_{-\infty}$ at which the velocities were set equal to the incoming Poiseuille flow values

$$(f_n = g_n = h_n = 0 \quad \text{except for} \quad f_0 = Y).$$

Typical x- and Y-mesh widths employed initially were $\Delta x = 0{\cdot}1$, $\Delta Y = 0{\cdot}25$. Trial calculations revealed however that a massive value of Y_∞ was needed to cope satisfactorily with the algebraic decay in (2.6*a*), (2.11)–(2.12), while simultaneously a fairly fine mesh spacing was necessary near the wall. Accordingly a stretched co-ordinate $\hat{Y}$ was introduced, defined by

$$Y = \hat{a}\hat{Y}(1+\hat{b}\hat{Y})/(1+\hat{d}\hat{Y})$$

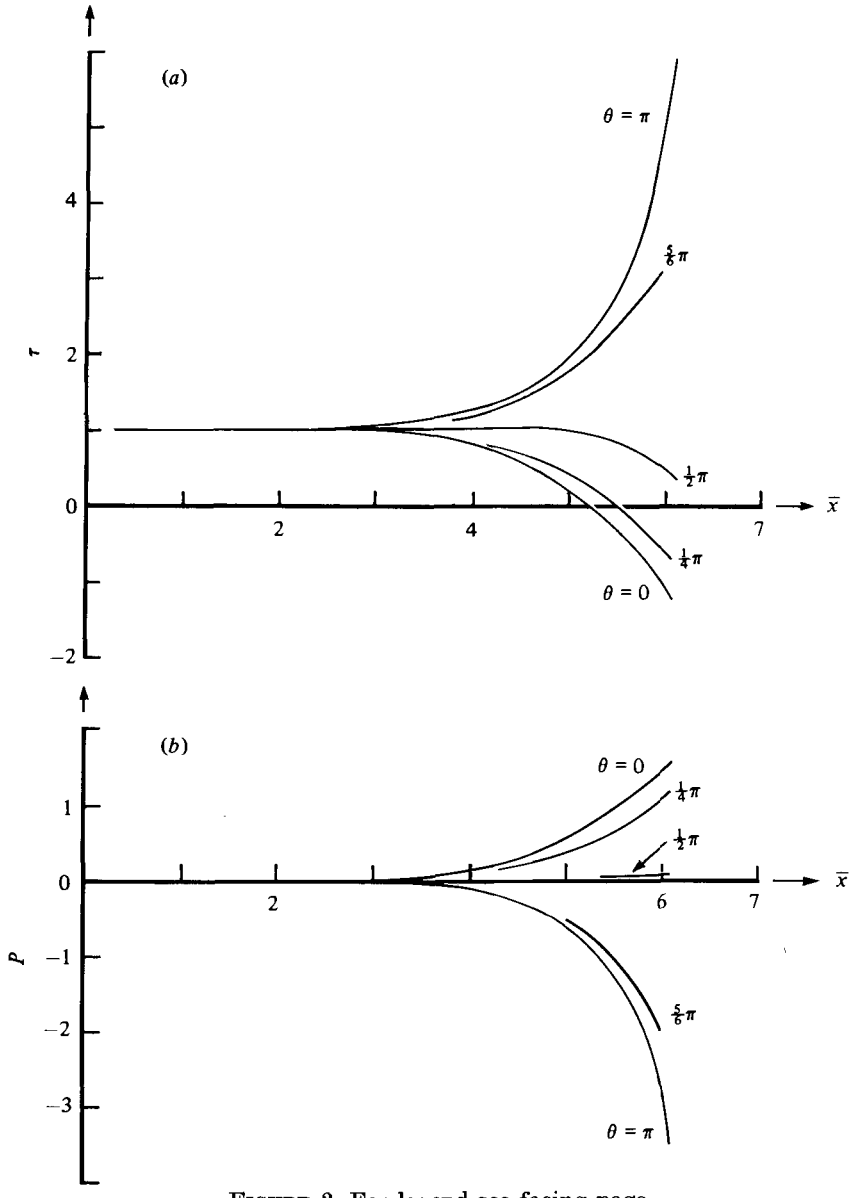

FIGURE 2. For legend see facing page.

and uniform steps $\Delta\hat{Y}$ in $\hat{Y}$ were taken. Typically the values $\Delta\hat{Y} = 0{\cdot}25$, $\hat{a} = 0{\cdot}2$, $\hat{b} = 1, \hat{d} = 0{\cdot}02$ were chosen, with 401 steps in $\hat{Y}$, so that the edge value $Y_\infty = 673{\cdot}3$ was achieved but with the smallest value of ΔY being 0·062... (next to the wall). The tolerance q was usually 10^{-7}, and we took $b_n = 0$ in (2.13) for all $|n| \neq 1$ in most calculations. Throughout the solutions the effects of changing Δx, $\Delta\hat{Y}$, Y_∞ or q were minimal. Doubling both the mesh widths Δx, $\Delta\hat{Y}$, but keeping Y_∞ fixed, altered the solutions for P by less than 0·002 %. Similarly, increasing Y_∞ to 1608 but keeping Δx, $\Delta\hat{Y}$ fixed yielded alterations of the order of 10^{-5} or less in the solutions. The effects of alterations in the values of M and b_n are commented on in § 3 below.

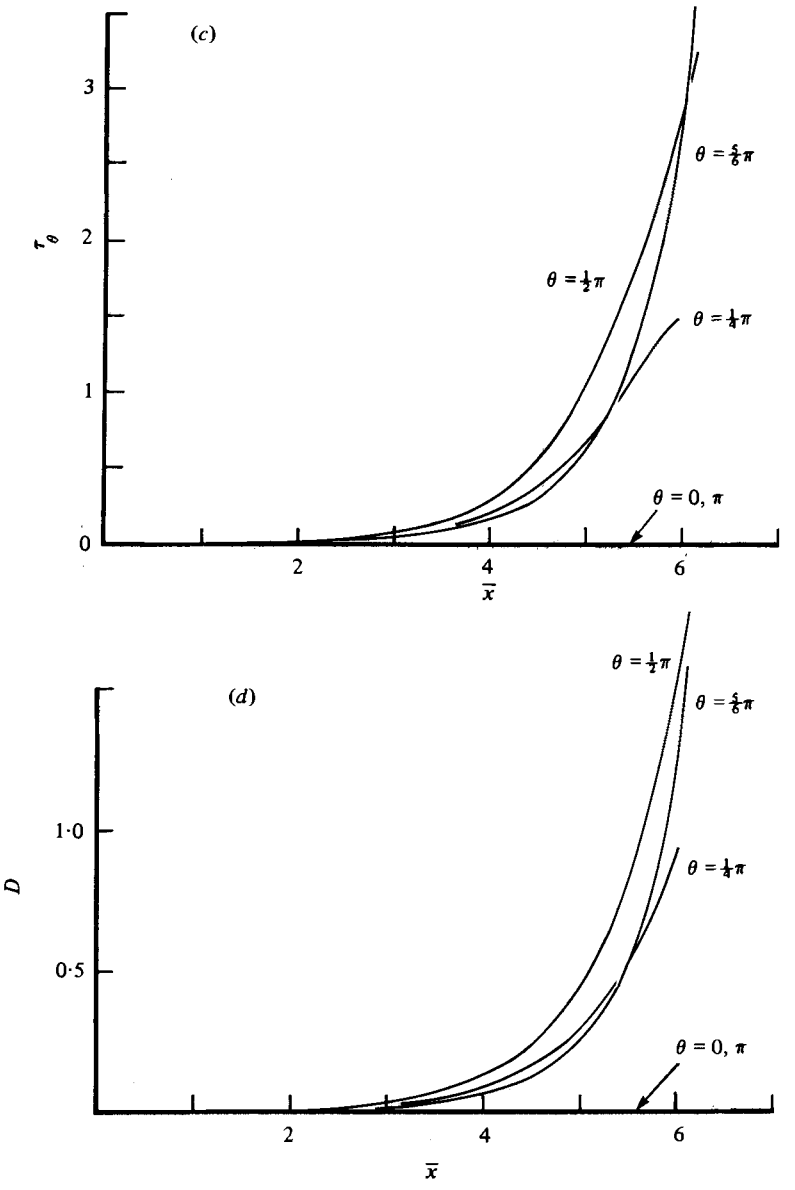

FIGURE 2. The calculated development with $\bar{x}$ ($\equiv x - x_{-\infty}$) of (*a*) the axial skin friction τ, (*b*) the pressure P, (*c*) the azimuthal skin friction τ_θ, (*d*) the azimuthal slip velocity D, for certain values of θ (case 1).

3. Numerical results

The program of § 2 was run for a number of different settings of the starting parameters b_n in (2.13) and the two solutions presented herein exhibit the properties typical of all the runs. First (case 1), we consider the solution developing from the initial setting $b_{\pm 1} = 0{\cdot}0005$ ($b_n = 0$ otherwise). Curves for the streamwise skin friction $\tau = (\partial U/\partial Y)\ (x, 0, \theta)$, pressure $P(x, \theta)$, azimuthal skin friction $\tau_\theta = (\partial W/\partial Y)\ (x, 0, \theta)$ and 'azimuthal slip velocity' $D(x, \theta)$ are given in figure 2. Good agreement is found

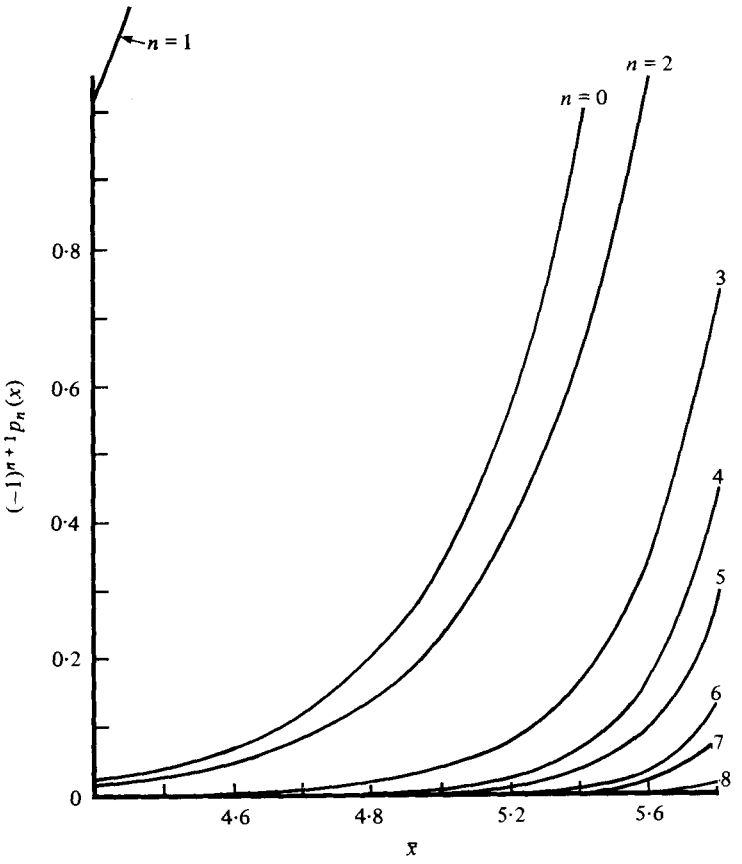

FIGURE 3. The calculated variation of the dominant Fourier components p_n (for $1 \leqslant n \leqslant 8$) of P with $\bar{x}$ $(= x - x_{-\infty})$ for case 1 (see (2.8a)).

between the numerical solutions and the proposed starting form (2.5) for small values of $\bar{x} \equiv (x - x_{-\infty})$. A numerical difficulty (described also by Sykes 1979) did arise, however, in the early trial calculations of the ensuing flow. For if M was set at a fairly low value (e.g. 4) then eventually a severe loss of resolution became apparent in the cross-flow (Y, θ) plane accompanied by divergence of the scheme. However, if M was set higher (e.g. 12) to avoid that problem then the unavoidable errors in the Mth Fourier components due to the series truncation always grew so rapidly (in a manner $(\propto e^{mx})$ akin to that of the terms $e^{mx}\cos m\theta$ implied in (2.5)) with increasing x, that marked loss of accuracy was again inevitable. The difficulty was overcome to a large extent simply by increasing the value of M gradually as x increased. In that way the influence of the higher-order Fourier components was suppressed (as it should be physically) until the flow became truly nonlinear and the interactions between the various Fourier modes could then yield the physically correct, non-violent, response in the higher-order modes. For the results shown in figure 2, for instance, we set $M = 6$ for $0 \leqslant x - x_{-\infty} < 4{\cdot}5$, and then increased M by 2 at each of the stations $x - x_{-\infty} = 4{\cdot}5$, 5·1, 5·7, 6·05 to finish with $M = 14$. It was found that such a treatment brought very good agreement (of the order of 10^{-6} in τ, P, τ_θ, D) with previous, constant M, treatments for $x - x_{-\infty}$ less than about 5·2 (near separation), beyond which station the

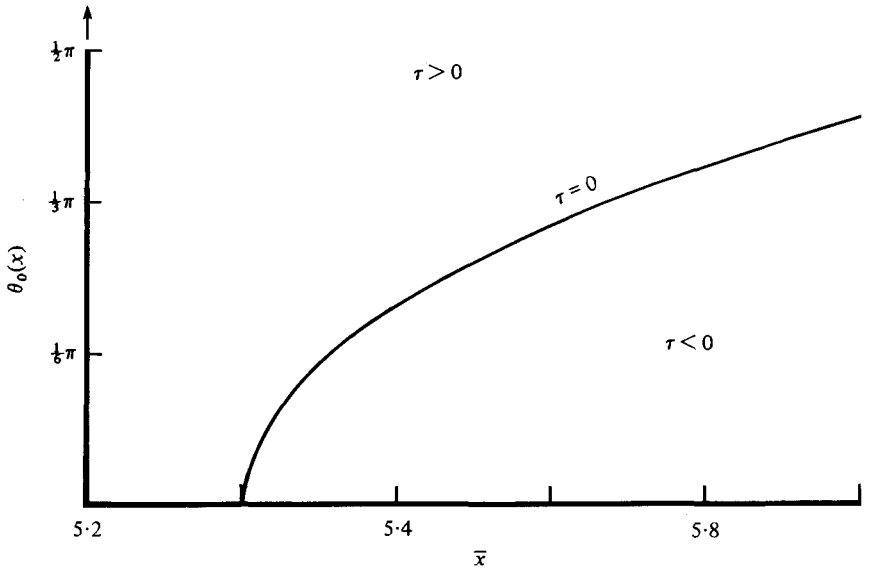

FIGURE 4. The separation curve $[\theta_0(x)$ versus $x - x_{-\infty}]$ on which $\tau = 0$, calculated for case 1. To the right of the curve the axial velocity U is reversed near the wall (see also figure 8).

constant M treatments soon diverged or lost accuracy, whereas the new treatment continued satisfactorily for a good distance beyond separation. The streamwise development (shown in figure 3) of the Fourier components of the pressure in figure 2 gives some indication of the above difficulty and its treatment by the variable M approach.

In the flow solutions of figure 2 the trend of the starting form (2.5) continues as the motion becomes ever more nonlinear, in that along $\theta = 0$ (the 'peak line') τ, $-P$, $-\partial\tau_\theta/\partial\theta$, $-\partial D/\partial\theta$ all continue to fall with increasing x, while they continue to rise along $\theta = \pi$ (the 'trough line'). In particular, separation (which we define here by $\tau = 0$) is eventually encountered on the peak line first, thereafter spreading out into the flow field to encompass a larger but limited range of values of θ. Figure 4 depicts the separation curve $\tau = 0$, $\theta = \theta_0(x)$, dividing the streamwise reversed flow region from the streamwise forward flow region. Beyond separation the forward marching numerical scheme of § 2 is open to question, of course, because of the sign reversal of U, but our solutions nevertheless continued on in an apparently sensible manner. No simple economic extension of the Reyhner & Flügge-Lotz (1968) approximation technique, or of Williams, (1975) decisive treatment for reversed flow, in two-dimensional boundary-layer problems, seemed feasible in our three-dimensional work, unfortunately, so that the downstream range of reversed flow covered by the calculations is not as long as might be desirable (see § 4 below, however). However, manipulation of the variable M scheme and reduction in the step size Δx if convergence was not obtained for a given step enabled the workings to proceed for an appreciable distance beyond separation. Indeed, the downstream integration range covered tended to be limited more by the vastness of the computer times required for iterative convergence than by divergence or loss of resolution in the numerical scheme. For example, up to 600 iterations per step were found necessary in the combined Newton and three-dimensionality iterative scheme to satisfy the $q = 10^{-7}$ tolerance near the end of the calculations.

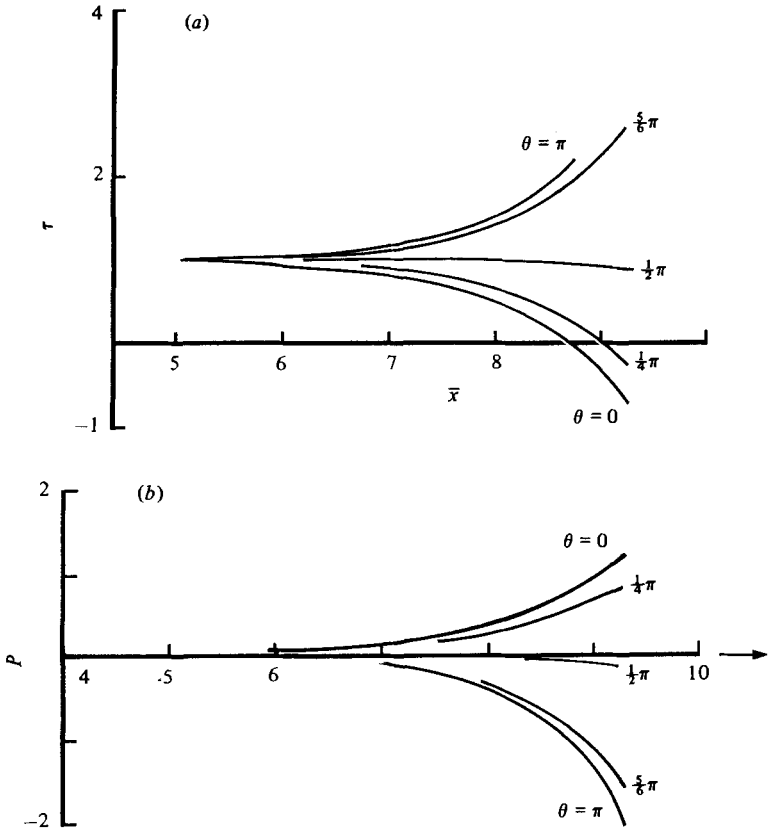

FIGURE 5. For legend see facing page.

As the separated flow zone increases downstream, by contrast the flow outside becomes increasingly attached to the wall with increasing x (see also figure 13 below). The growth with x of τ, $-\partial\tau_\theta/\partial\theta$, $-P$ and $-D$ outside is in fact much more pronounced than the fall in those quantities inside the separated flow zone. The physical explanation of this continuation of the initial trend in (2.5) is similar to that of Smith (1976*b*). The pressure rise along the peak line provokes separation and so the boundary layer is pushed away ('upward') from the wall there; but the lack of displacement then turns this upward movement into a sideways (θ) one; and the sideways flow therefore enhances the effect of the favourable pressure gradient in the θ direction produced by the pressure rise in the peak line and supports the strong attachment phenomenon around the trough line. Beyond separation the adverse axial pressure gradient within the separated zone is relatively mild, but enough to maintain the relatively slow reversed flow there.

The second solution presented here, case 2, for which $b_{\pm1} = 0{\cdot}00005$ ($b_n = 0$ otherwise) in (2.13), exhibits similar characteristics (figures 5–8). It should be emphasized, however, that this different choice for $b_{\pm1}$ does yield a genuinely different flow solution from that of case 1. This is because of the three-dimensionality of the initial form (2.5) and its subsequent nonlinear development. By contrast, in previous two-dimensional work (e.g. Stewartson & Williams 1969; Smith & Stewartson 1973*a*, *b*; Smith & Duck 1977) on free interactions, a change in the (single) initial arbitrary pressure constant

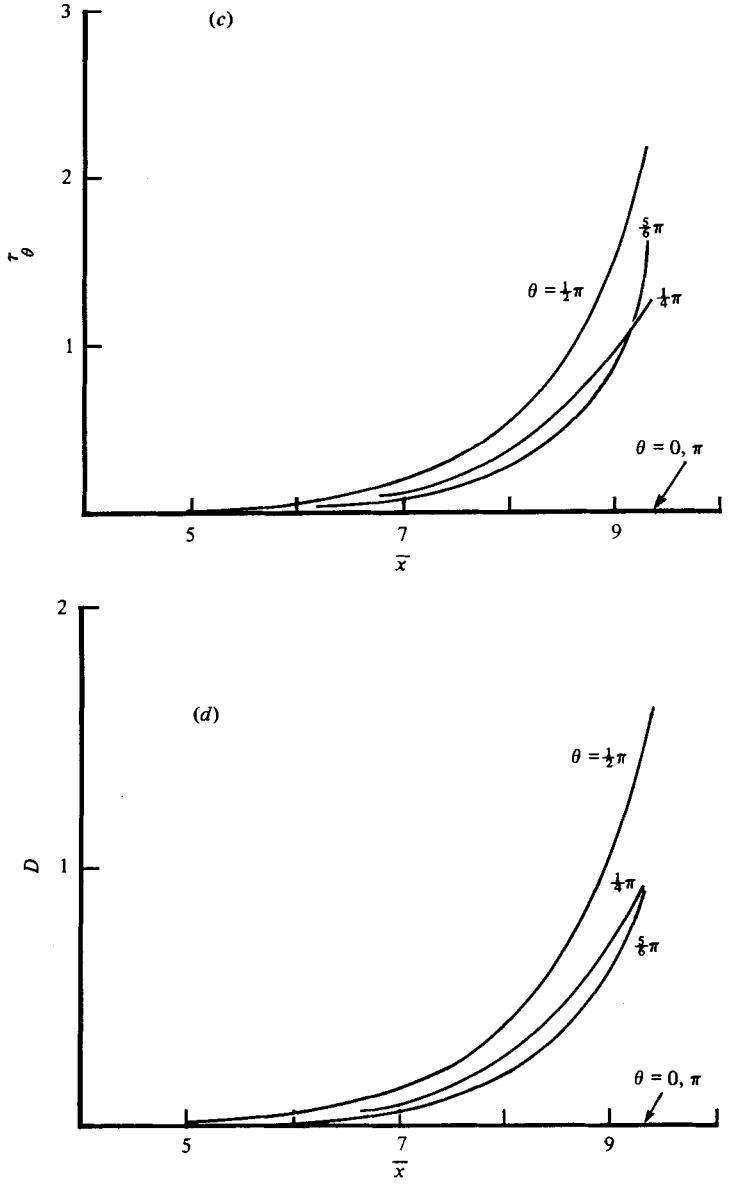

FIGURE 5. The calculated variation with $\bar{x} = x - x_{-\infty}$ of (*a*) the axial skin friction τ, (*b*) the pressure P, (*c*) the azimuthal skin friction τ_θ, (*d*) the azimuthal slip velocity D, for certain values of θ (case 2).

merely causes an origin shift in the otherwise unique free interaction. No such simple interpretation holds in the three-dimensional boundary layer, for there are infinitely many free interactions possible corresponding to the infinity of choices possible for the constants b_n in (2.13). For case 2 figure 5 presents the streamwise variation of τ, P, τ_θ, D, while figures 6, 7 give the separation curve ($\theta = \theta_0(x)$) and a series of velocity profiles respectively. Figure 7, in particular, confirms the strong attachment phenomenon outside the separation zone and within the separation zone gives an appearance increasingly resembling that of a classical vortex sheet (see J. H. B. Smith 1975) as x

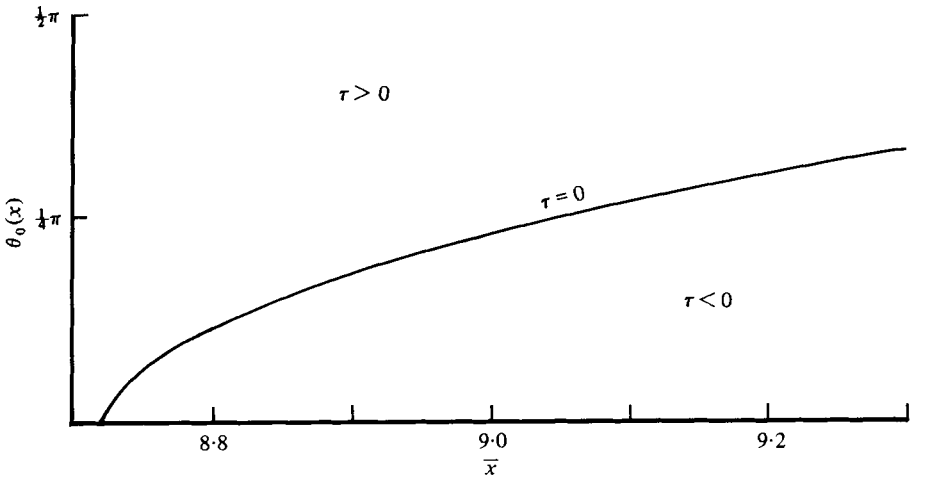

FIGURE 6. The separation curve for case 2 (see comments for figure 4).

increases. Finally, in figure 8 are drawn the curves on which $U = 0$ in cross-flow planes beyond separation.

In § 4 we move on to consider the ultimate form of the three-dimensional free interaction solutions.

4. On the termination of the upstream response and the formation of a vortex sheet

Our task is to describe the typical ultimate behaviour of solutions to (2.2*a–c*), (2.3*a*, *b*), (2.6*a*, *b*), (2.7) downstream. Some hints on the asymptotic structure are given by the numerical solutions of § 3 of course, but the major need in the asymptotic structure is for overall self-consistency. Initially, bearing in mind the downstream asymptotic work of Stewartson & Williams (1973), Smith (1976*a*), Smith & Duck (1977) in different two-dimensional flow studies, we postulated an algebraic behaviour as $x \to \infty$ (for fixed θ). However, close inspection of the attached part of the flow field led us to the conclusion that such an ultimate form is unlikely there because no sensible balance can be struck between the inertial and pressure forces in the momentum equations, or between the three components of the continuity equation, in (2.2). Instead the axial pressure gradient tends to be suppressed in such an algebraic asymptotic form. With the absence (to leading order) of the axial pressure gradient a satisfactory account of the attached part proved impossible to find. The conclusion that the attached part of the flow field does not admit of an algebraic description as $x \to \infty$ can be reinforced by examining the motion near the trough line $\theta = \pi$ (in similar fashion to (4.1)–(4.10) below).

Again, the possibility (raised by the results in figures 2–10) of an exponential behaviour of the free interaction as $x \to \infty$ also seemed to be ruled out because of similar difficulties. In fact, verification of the failure of the above two forms may be derived from the work in § 4.1 below.

The above difficulties led us to test, next, the possibility of an algebraically singular termination of the free interaction at a finite line, $x = x_0(\theta)$ say. This postulate

appeared to offer a not inconsistent description of the attached flow part (A), and its features are set out below in §4.1. On the other hand no such algebraic singularity provided a satisfactory description for the ultimate separated flow zone (B) near $\theta = 0$ and only a certain algebraic behaviour as $x \to \infty$, with the pressure tending to a constant plateau value over the entire separated flow zone, enabled a self-consistent account of the latter zone to be made. Consequently we believe that the singular line $x = x_0(\theta)$ cannot extend right across the flowfield, from the trough line to the peak line, and that instead it must sweep to downstream infinity (figure 9) at some value of θ between 0 and π. Other possible forms for the behaviour of the singular line can be raised of course, but a combination of the evidence from the full calculations of §3 and the analysis near the peak line $\theta = 0$ (§4.2 below) implies a sweeping downstream without reaching the peak line, while physical sense tends to suggest our looking for the simplest such sweep. So our analytic discussion of the ultimate behaviour of the three-dimensional flow solution will be split into two distinct parts in §4.1, 4.2 below.

4.1. *The ultimate attached flow zone* (A)

We propose, then, that the attached part A of the flow field for $x \to x_0(\theta)-$ is defined by $\gamma_0 < \theta \leqslant \pi$, where $x_0(\theta) \to \infty$ as $\theta \to \gamma_0+$ (figure 9), and by symmetry

$$x_0(\theta) \sim x_0(\pi) + O(\pi-\theta)^2 \quad \text{as} \quad \theta \to \pi-.$$

Introducing $X \equiv x_0(\theta) - x$ and $\overline{U} \equiv U - x_0'(\theta)\, W$ for convenience, so that the controlling equations (2.2) become

$$-\overline{U}_X + V_Y + W_\theta = 0, \tag{4.1a}$$

$$-\overline{U}\overline{U}_X + V\overline{U}_Y + W\overline{U}_\theta + x_0''(\theta)\, W^2 = (1+x_0'^2)\, P_X + x_0'(\theta)\, P_\theta + \overline{U}_{YY}, \tag{4.1b}$$

$$-\overline{U}W_X + VW_Y + WW_\theta = -P_\theta - x_0'(\theta)\, P_X + W_{YY} \tag{4.1c}$$

(subscripts and primes denoting derivatives where appropriate), we seek the solution of (4.1a–c) [and the appropriate boundary conditions stemming from (2.3a, b), (2.6a, b), (2.7)] for $0 < X \ll 1$. In fact the only part of A that admits at all readily of a convincing analysis is the neighbourhood of the trough line, $\theta \to \pi$, where W must vanish. The vanishing of W at $\theta = \pi$ is achieved via the region wherein $(\pi - \theta)$ and X are both small and comparable (in order that the axial and azimuthal pressure gradients may interact, cf. first paragraph of §4). Setting $\pi - \theta = \overline{\theta} X$, with $\overline{\theta}$ of $O(1)$, then, we try the singular form

$$P(x, \theta) \sim \tilde{P}(\overline{\theta})\, X^{-2N} \tag{4.2}$$

for $X \to 0$, where the constant $N(>0)$ and function $\tilde{P}(\overline{\theta})$ are unknown. The flow field for $\overline{\theta} = O(1)$ then subdivides into an outer inviscid zone $A1$, to satisfy (2.6a, b), and a viscous wall layer $A2$, driven by the slip velocity induced in $A1$ and required to satisfy the no-slip conditions.

In $A1$, Y is large [$Y = X^{-N}\eta$ with η of $O(1)$] and

$$(\overline{U}, V, W) = (X^{-N}\tilde{F}(\eta, \overline{\theta}),\ X^{-2N-1}\tilde{G}(\eta, \overline{\theta}),\ X^{-N}\tilde{H}(\eta, \overline{\theta})) \tag{4.3}$$

to leading order. From (4.1), $\tilde{F}$, $\tilde{G}$, $\tilde{H}$, $\tilde{P}$ satisfy the inviscid nonlinear equations

$$\left.\begin{aligned} &N\tilde{F} - N\eta\tilde{F}_\eta + \overline{\theta}\tilde{F}_{\overline{\theta}} + \tilde{G}_\eta - \tilde{H}_{\overline{\theta}} = 0, \\ &\tilde{F}(N\tilde{F} - N\eta\tilde{F}_\eta + \overline{\theta}\tilde{F}_{\overline{\theta}}) + \tilde{G}\tilde{F}_\eta - \tilde{H}\tilde{F}_{\overline{\theta}} - = -2N\tilde{P} - \overline{\theta}\tilde{P}'(\overline{\theta}), \\ &\tilde{F}(N\tilde{H} - N\eta\tilde{H}_\eta + \overline{\theta}\tilde{H}_{\overline{\theta}}) + \tilde{G}\tilde{H}_\eta - \tilde{H}\tilde{H}_{\overline{\theta}} = \tilde{P}'(\overline{\theta}), \end{aligned}\right\} \tag{4.4a}$$

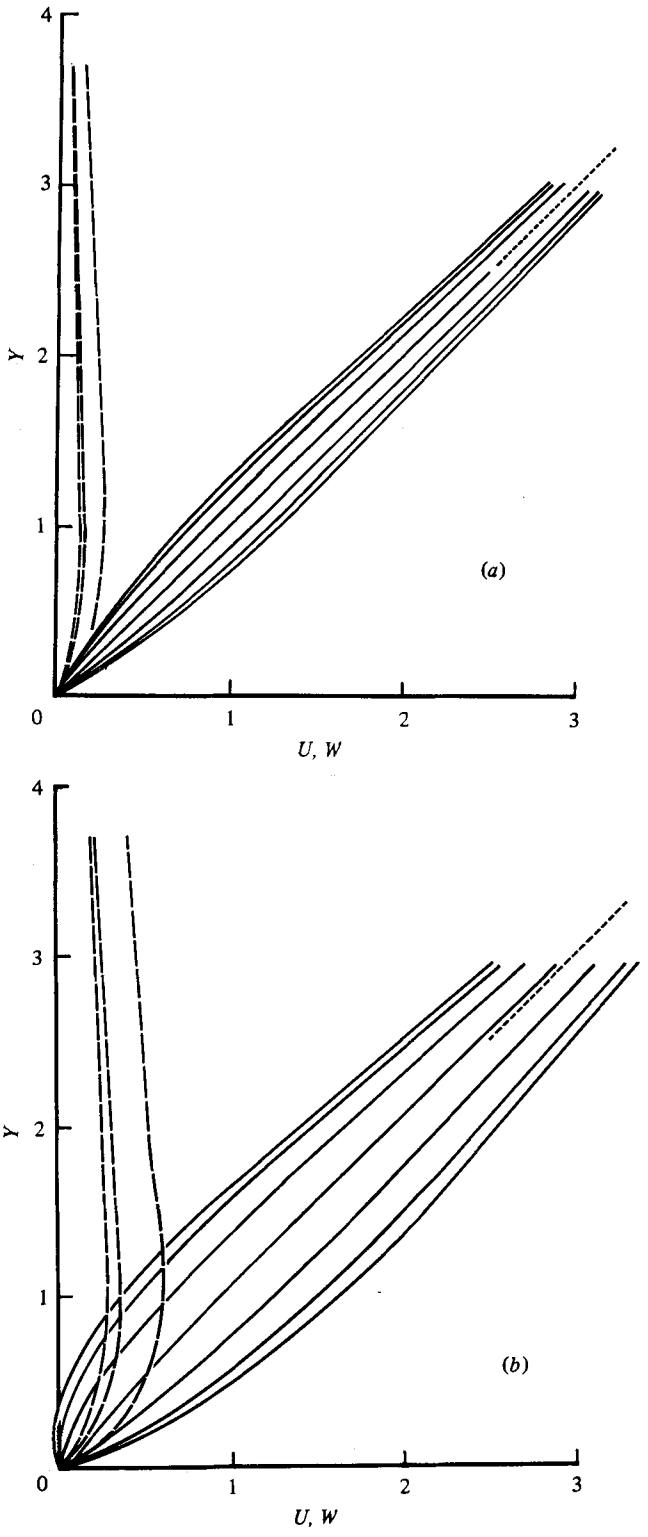

FIGURE 7. For legend see facing page.

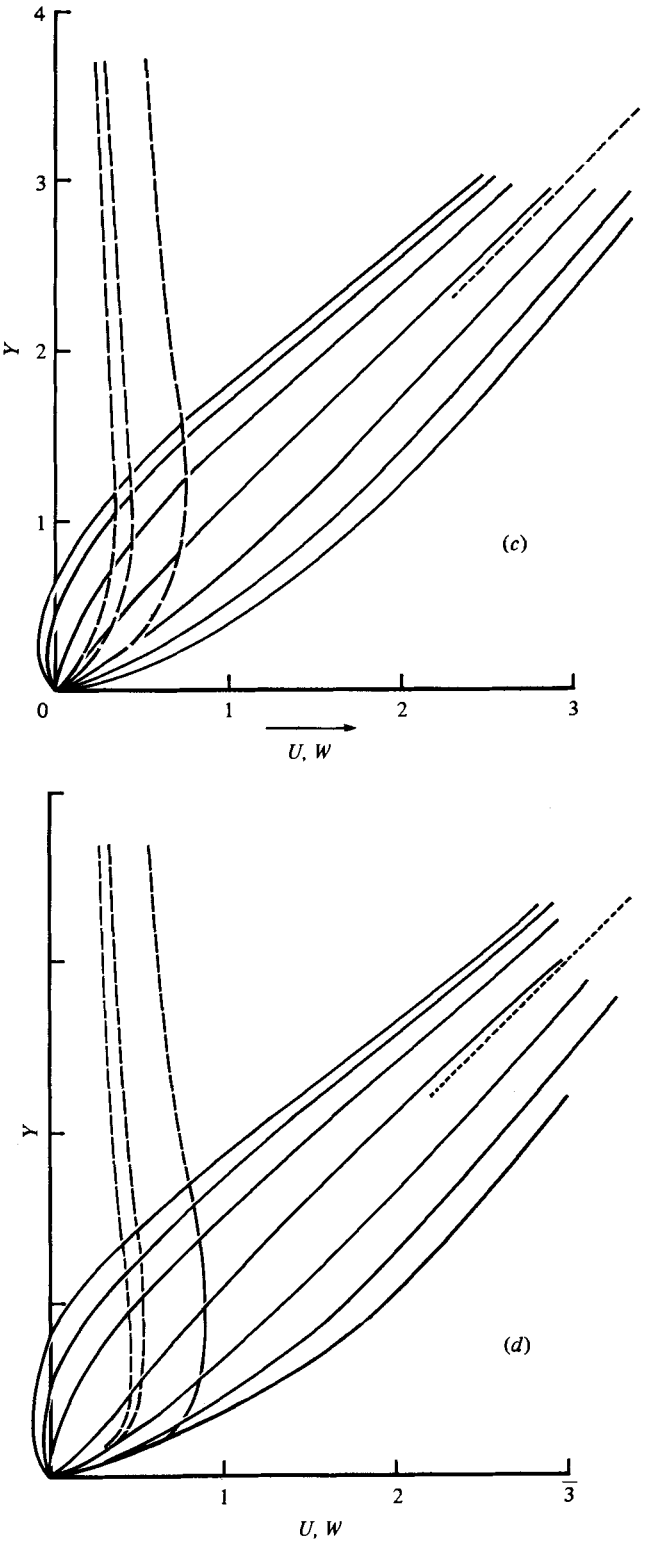

FIGURE 7. Calculated velocity profiles U, W verses Y, at various values of θ, for case 2 at (*a*) $\bar{x} = 8{\cdot}2$, (*b*) $\bar{x} = 9{\cdot}0$, (*c*) $\bar{x} = 9{\cdot}2$, (*d*) $\bar{x} = 9{\cdot}3$, where $\bar{x} = x - x_{-\infty}$. The solid curves give U at (from left to right) $\theta = 0, \frac{1}{6}\pi, \frac{1}{3}\pi, \frac{1}{2}\pi, \frac{2}{3}\pi, \frac{5}{6}\pi, \pi$; the dashed curves give W at (from left to right) $\theta = \frac{1}{6}\pi, \frac{5}{6}\pi, \frac{1}{2}\pi$; and the dotted line indicates the asymptote (2.3*b*) for U as $Y \to \infty$.

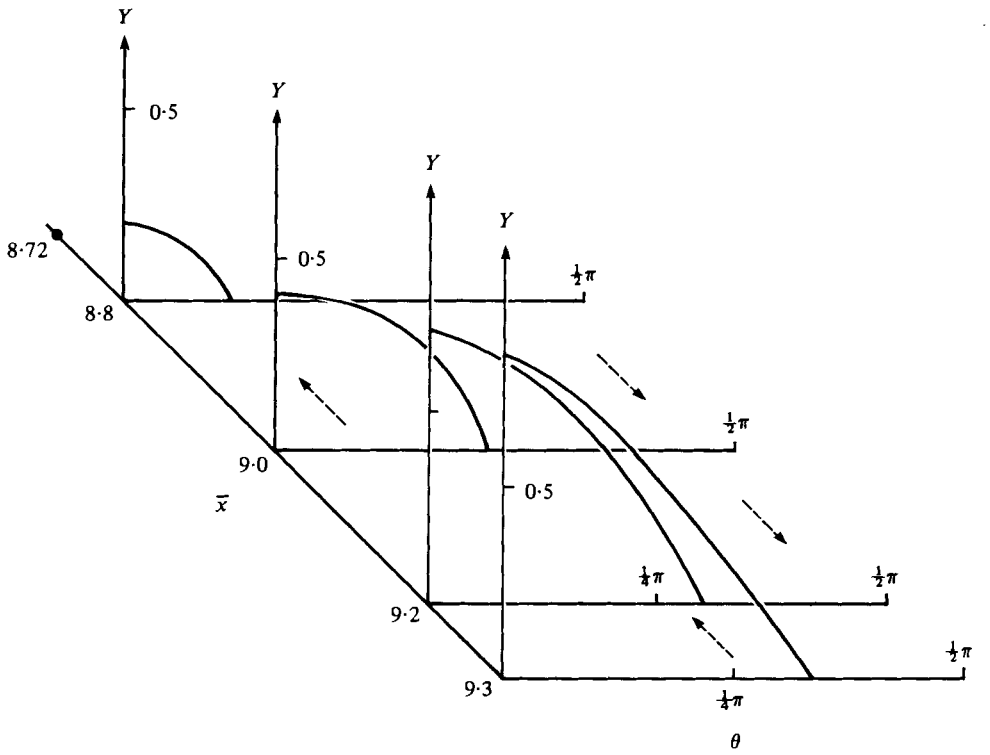

FIGURE 8. The calculated curves of zero streamwise velocity ($U = 0$) in the cross-flow (Y, θ) plane (case 2), at the $\bar{x}(= x - x_{-\infty})$ stations shown. The figure is meant to convey the streamwise development of the reversed flow zone, with the dashed arrows indicating the axial flow directions.

and the outer constraints (from (2.6a))

$$\tilde{F} \sim \eta + O(\eta^{-1}), \quad \tilde{G} \to O(1), \quad \tilde{H} \sim O(\eta^{-1}) \quad \text{as} \quad \eta \to \infty, \tag{4.4b}$$

while as $\eta \to 0+$ we expect the tangential flow properties

$$\tilde{F} \to \tilde{F}_0(\bar{\theta}), \quad \tilde{G} \sim O(\eta), \quad \tilde{H} \to \tilde{H}_0(\bar{\theta}) \tag{4.4c}$$

to hold. Here the unknown slip velocities $\tilde{F}_0(\bar{\theta})$, $\tilde{H}_0(\bar{\theta})$ satisfy the relations

$$N\tilde{F}_0^2 + \bar{\theta}\tilde{F}_0\tilde{F}_0' - \tilde{H}_0\tilde{F}_0' = -2N\tilde{P} - \bar{\theta}\tilde{P}', \quad N\tilde{F}_0\tilde{H}_0 + \bar{\theta}\tilde{F}_0\tilde{H}_0' - \tilde{H}_0\tilde{H}_0' = \tilde{P}' \tag{4.4d}$$

from (4.4a) (at $\eta = 0$). End conditions, at $\bar{\theta} = 0$ and $\bar{\theta} \to \infty$, are also required and these are discussed later.

In the viscous wall layer, $A2$, Y is small, with $\xi = YX^{-\frac{1}{2}-\frac{1}{2}N}$ of $O(1)$, and to leading order

$$(\bar{U}, V, W) = (X^{-N}F(\xi, \bar{\theta}), X^{-\frac{1}{2}-\frac{1}{2}N}G(\xi, \bar{\theta}), X^{-N}H(\xi, \bar{\theta})). \tag{4.5}$$

Here from (4.1) $F, G, H, \tilde{P}$ satisfy the viscous equations

$$\left.\begin{aligned} &NF + \tfrac{1}{2}(N+1)\xi F_\xi + \bar{\theta}F_{\bar{\theta}} + G_\xi - H_{\bar{\theta}} = 0, \\ &F[NF + \tfrac{1}{2}(N+1)\xi F_\xi + \bar{\theta}F_{\bar{\theta}}] + GF_\xi - HF_{\bar{\theta}} = -2N\tilde{P} - \bar{\theta}\tilde{P}'(\bar{\theta}) + F_{\xi\xi}, \\ &F[NH + \tfrac{1}{2}(N+1)\xi H_\xi + \bar{\theta}H_{\bar{\theta}}] + GH_\xi - HH_{\bar{\theta}} = \tilde{P}'(\bar{\theta}) + H_{\xi\xi}, \end{aligned}\right\} \tag{4.6a}$$

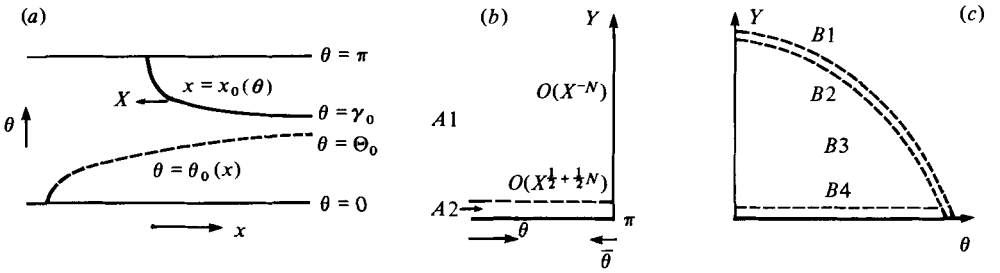

FIGURE 9. (*a*) The proposed structure of the flowfield downstream, showing the terminal singular curve (studied in §4.1), the separation curve (see §4.2) and notation used. (*b*) The theoretical, attached flow, structure near $x = x_0(\pi)$ (§4.1). (*c*) The theoretical, separated flow, structure as $x \to \infty$ (§4.2).

with the boundary conditions of no slip at the wall and, for $\xi \to \infty$, merging with $A1$,

$$\left.\begin{aligned} &F = G = H = 0 \quad \text{at} \quad \xi = 0, \\ &F \to \tilde{F}_0(\bar{\theta}), \quad H \to \tilde{H}_0(\bar{\theta}) \quad \text{as} \quad \xi \to \infty. \end{aligned}\right\} \tag{4.6b}$$

End conditions are also required in zone $A2$.

Complete solutions for zones $A1$, $A2$ have not been attempted yet. For even the local solution near the trough line leads to many complications, as follows. As $\bar{\theta} \to 0$ ($\theta \to \pi - o(X)$) we anticipate the behaviour

$$(\tilde{F}, \tilde{G}, \tilde{H}, \tilde{P}) \sim (\mathscr{F}(\eta), \mathscr{G}(\eta), \bar{\theta}\mathscr{H}(\eta), -P_0 + \bar{\theta}^2 P_2) \tag{4.7}$$

in $A1$, where the non-zero constants P_0, P_1 are expected to be positive. Substitution into (4.4*a*, *b*) then yields the problem

$$N(\mathscr{F} - \eta\mathscr{F}') + \mathscr{G}' - \mathscr{H} = 0, \tag{4.8a}$$

$$N\mathscr{F}(\mathscr{F} - \eta\mathscr{F}') + \mathscr{G}\mathscr{F}' = 2NP_0, \tag{4.8b}$$

$$\mathscr{F}[(N+1)\mathscr{H} - N\eta\mathscr{H}'] + \mathscr{G}\mathscr{H}' - \mathscr{H}^2 = 2P_2, \tag{4.8c}$$

with

$$\mathscr{F} \sim \eta + \frac{P_2}{N(2N+1)\eta} + O(\eta^{-3}), \quad \mathscr{G} \to 2NP_0 - \frac{2P_2}{2N+1}, \quad \mathscr{H} \sim \frac{2P_2}{(2N+1)\eta} + O(\eta^{-3})$$
$$\text{as} \quad \eta \to \infty \tag{4.8d}$$

for $\mathscr{F}$, $\mathscr{G}$, $\mathscr{H}$. This nonlinear problem can be solved by substituting for $\mathscr{G}$, $\mathscr{H}$ from (4.8*a*, *b*) into (4.8*c*), to yield a nonlinear ordinary differential equation for $\mathscr{F}(\eta)$ alone, and then regarding $d\mathscr{F}/d\eta$ as a function of $\mathscr{F}$ in that equation. After manipulation and introducing thevariables $\zeta = (2P_0)^{-\frac{1}{2}}\mathscr{F}$, $Q = (\zeta^2 - 1)^{-([N+1]/4N)} d\mathscr{F}/d\eta$ and the constant $\kappa = P_2/P_0$, the associated Legendre equation (see, for example, Hobson 1931),

$$(1-\zeta^2)Q'' - 2\zeta Q' + \left[\left(\frac{1-N^2}{4N^2}\right) - \frac{\{\frac{1}{4}(N+1)^2 - \kappa\}}{N^2(1-\zeta^2)}\right] Q = 0, \tag{4.9a}$$

for $Q(\zeta)$ is obtained with the boundary condition

$$\zeta^{\frac{1}{2}+1/2N} Q \to 1 \quad \text{as} \quad Q \to \infty \tag{4.9b}$$

(from (4.8*d*)). This condition is enough to fix the solution of (4.9*a*) uniquely for arbitrary positive values of κ, N provided only that $\kappa < \frac{1}{4}(N+1)^2$. However, an additional

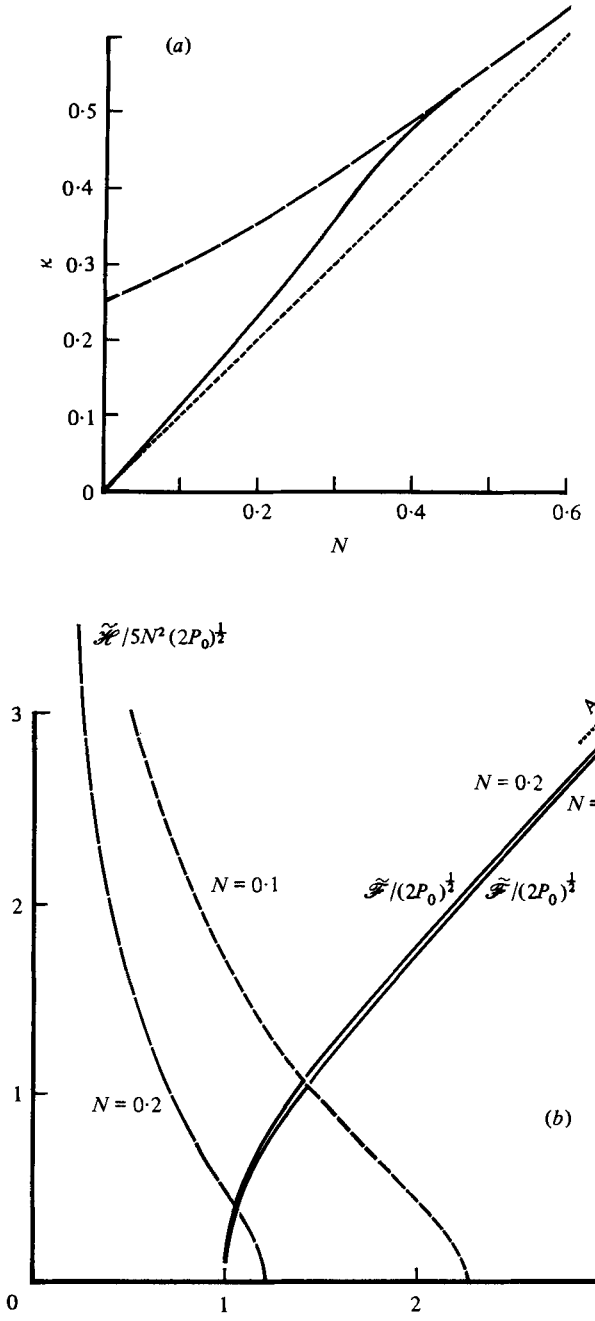

FIGURE 10. (*a*) The solid curve gives the calculated variation of the values $\kappa = \kappa_1(N)$ on which (4.9*a–c*) is satisfied, while for comparison purposes the dashed curve gives the boundary $\kappa = \frac{1}{4}(N+1)^2$ and the dotted line gives $\kappa = N$ (cf. (4.13)–(4.18)). (*b*) The theoretical velocity profiles $\tilde{\mathscr{F}}$, $\tilde{\mathscr{H}}$ [according to (4.7)–(4.9)] as functions of η, for the particular values $N = 0{\cdot}1$, $N = 0{\cdot}2$ along the curve $\kappa = \kappa_1(N)$ of figure 10(*a*).

constraint is necessary to ensure the tangential flow condition at the wall, $\mathscr{G}(0) = 0$ (or, equivalently, that $\zeta = 1$ at $\eta = 0$), namely

$$\int_1^\infty \frac{(\zeta^2-1)^{-\frac{1}{2}-1/4N}}{Q(\zeta)}\,d\zeta = 1. \tag{4.9c}$$

The integral condition (4.9*c*) is satisfied only when κ is a certain function ($\kappa_1(N)$) of N. For example, when N is small the solution of (4.9*a–c*) is

$$Q(\zeta) = (\zeta^2-1)^{-1/4N+\frac{1}{2}}[\zeta^{-1}+N\{\zeta^{-3}+\tfrac{1}{2}\zeta^{-1}\ln(1-\zeta^{-2})\}+O(N^2)] \tag{4.10a}$$

for $\infty > \zeta - 1 \gg \exp(-N^{-1})$, and

$$\kappa = N + N^2 + O(N^3). \tag{4.10b}$$

Further, it can be shown analytically that the solution of (4.9*a–c*) exists for $0 < N < \frac{1}{3}$ but does not exist for $N > \frac{1}{2}$. In general, however, to find $\kappa = \kappa_1(N)$ satisfying (4.9*a–c*) a numerical solution is necessary. This was obtained by using the series (in inverse powers of ζ) satisfying (4.9*a*, *b*) for a given value of N and κ, calculating the left-hand side of (4.9*c*) and iterating with κ until (4.9*c*) was satisfied. The effects of the number of terms (up to 800) taken in the series solution and of the number of steps (up to 200) employed in the integration in (4.9*c*) were investigated and led to an estimated error of $\frac{1}{2}$ % in κ_1 for a given N. Comparisons were made with analytical results obtainable for $N = 1, \frac{1}{2}, \frac{1}{3}$ and $N \to 0$ (see (4.10*a*, *b*)) and these confirmed the accuracy of the numerical method. The curve $\kappa = \kappa_1(N)$ upon which (4.9*a–c*) are satisfied is drawn in figure 10, along with corresponding velocity profiles at two representative points along the curve. We note that

$$\mathscr{H}(0) = (2P_0)^{\frac{1}{2}}\{\tfrac{1}{2}(N+1) - [\tfrac{1}{4}(N+1)^2 - \kappa]^{\frac{1}{2}}\} \tag{4.10c}$$

and that $\kappa_1 > N$ throughout.

For a self-consistent account of the motion near the trough line it is vital that we demonstrate the existence of a solution for the viscous wall layer $A2$ on at least one point of the curve $\kappa = \kappa_1(N)$. Since the streamwise and azimuthal pressure gradients are favourable, initially one might expect a viscous solution to exist for all $\kappa = \kappa_1(N)$ but in fact the situation is more involved than that, as the analysis below shows. In $A2$ we expect the behaviour

$$(F, G, H) \sim (\mathscr{F}(\xi), \mathscr{G}(\xi), \bar{\theta}\mathscr{H}(\xi)) \quad \text{as} \quad \bar{\theta} \to 0+. \tag{4.11}$$

We then set $S(\hat{\xi}) = (2P_0)^{-\frac{1}{2}}\mathscr{F}$, $T'(\hat{\xi}) = (2P_0)^{-\frac{1}{2}}[\mathscr{H} + \frac{1}{2}(1-N)\mathscr{F}]$, $\hat{\xi} = (2P_0)^{\frac{1}{2}}\xi$ for convenience, which, from (4.6*a*, *b*), lead to the nonlinear similarity problem

$$S'' - TS' + N(1-S^2) = 0, \tag{4.12a}$$

$$T''' - TT'' + T'^2 - 2T'S + \tfrac{1}{4}S^2(1-N)(3-N) + \kappa + \tfrac{1}{2}N(1-N) = 0, \tag{4.12b}$$

with

$$T(0) = T'(0) = S(0) = 0, \tag{4.12c}$$

$$S(\infty) = 1, \quad T'(\infty) = 1 - [\tfrac{1}{4}(N+1)^2 - \kappa]^{\frac{1}{2}}. \tag{4.12d}$$

Here the minus sign for the square root in (4.12*d*) (as in (4.10*c*)) follows from the behaviour of $Q(\zeta)$ as $\zeta \to 1+$ in (4.9*a–c*) and from (4.4*d*). We note that S, T' tend to their asymptotic values in (4.12*d*) in an algebraic fashion.

The problem (4.12*a–d*) is reminiscent of the similarity problems arising in rotating fluids (see Rott & Lewellen's 1966 review and the pioneering work of Belcher, Burggraf & Stewartson (1972)), but (4.12*a–d*) is of a type apparently not studied previously. Our initial attempts at finding numerical solutions to (4.12*a–d*) for values of κ, N along the curve $\kappa = \kappa_1(N)$ proved inconclusive and raised severe doubts about the existence of solutions in the required regime. It was decided, therefore, that a broader study of the properties of (4.12*a–d*) was necessary, to establish the existence or not of solutions along $\kappa = \kappa_1(N)$. Further, the relative lack of knowledge of similarity solutions for general three-dimensional boundary layers suggests that a detailed examination of the similarity problem (4.12*a–d*) is warranted from a more general viewpoint in any case. Our approach is as follows.

First, relatively simple solutions of (4.12*a–d*) exist for $\kappa = 0$ provided $0 < N \leqslant 1$. These are two-dimensional flow solutions in which $\frac{1}{2}(1-N)S = T'$ and $T(\xi)$ satisfies the Falkner–Skan problem with, in the notation of Jones & Watson (1963), $\alpha = -1$ and $\beta > 0$. It can be shown further that regular (three-dimensional) perturbations from these solutions are possible when κ is small. This last property would be useful in three-dimensional triple-deck flow studies involving singularities; Stewartson's (1971) singularity for two-dimensional flow corresponds to our value $N = 1$ at $\kappa = 0$. Secondly, a Falkner–Skan solution is also obtained for $\kappa = N$ when $N \geqslant 1$, since then $S = 2T'/(1+N)$. However, perturbations from the solution at $\kappa = N = 1$ are possible when $(\kappa - 1)$, $(N-1)$ are both small only if κ lies below the line $\kappa = N$ (see appendix). Thirdly, it is readily shown that no solution of (4.12*a–d*) exists at $N = 0$ if $\kappa > 0$, and, further, no self-consistent structure for a solution when $N \to 0+$ with $\kappa > 0$ seems forthcoming. Fourthly, numerical solutions were obtained for a number of values of κ by letting N decrease from 1. The numerical scheme used central differencing and Newton iteration, and the effects of the calculation range and step size were tested for all the solutions: indeed, such tests were vital in deciding the solution properties, both because of the sensitive nature of the algebraic decay as $\xi \to \infty$ and because of the thickening of the wall layer when $\kappa, N \to 0$ (cf. the splitting of the Falkner–Skan solutions for $\alpha = -1$, $\beta > 0$ when $\beta \to 0$; see appendix). Sample results, all with $\kappa < N$, are shown in figure 11 (*a*, *b*). Their outstanding properties are the overshoot in T', which occurs and becomes accentuated as N decreases from unity, and the thickening of the wall layer with decreasing N. A plot of the maximum ($T'_{\max}$) of T' against N, for given κ, is given in figure 11 (*c*). Most importantly, the evidence from figure 11 (*c*) and the fact that solutions could not be obtained for $\kappa = N$ raise the possibility that the solution of (4.12*a–d*) is singular along $\kappa = N$. The following analysis (cf. Belcher *et al.* 1972) confirms the existence of a singular structure when $(\kappa - N)$ is small, and indeed shows that solutions *are* possible for some values of $\kappa > N$.

Suppose $\kappa = N_0 + \bar{\kappa}\epsilon$, $N = N_0 + \bar{N}\epsilon$, where $\bar{\kappa}$, $\bar{N}$, N_0 are $O(1)$ but

$$0 < \epsilon \ll 1 \quad \text{and} \quad 0 < N_0 < 1.$$

The solution of (4.12*a–d*) then subdivides into two zones, $Z1$ and $Z2$. In $Z1$, where ξ is $O(1)$, the wall conditions are to be satisfied, whereas the outer conditions (4.12*d*) are unattainable. The solution then adjusts to the conditions (4.12*d*) in zone $Z2$, where $\xi \gg 1$. Specifically, in $Z1$

$$S = S_0 + \epsilon S_1 + \ldots, \quad T = T_0 + \epsilon T_1 + \ldots \tag{4.13}$$

with $T_0' = \frac{1}{2}(3-N_0)S_0$. Here $S_0 \to 1$ as $\hat{\xi} \to \infty$, so that the outer condition on T' in (4.12*d*) ($T' \to \frac{1}{2}(1+N_0)$) is not satisfied. However, (4.12*a*, *b*) now become identical and from the leading terms in (4.12*a*–*c*) T_0 satisfies the Falkner–Skan problem

$$T_0''' - T_0 T_0'' + \frac{N_0(3-N_0)}{2}\left[1 - \left(\frac{2}{3-N_0}\right)^2 T_0'^2\right] = 0, \tag{4.14a}$$

$$T_0(0) = T_0'(0) = 0, \quad T_0'(\infty) = \left(\frac{3-N_0}{2}\right), \tag{4.14b}$$

the solution of which exists for $3 > N_0 > 0$. The next-order terms then leave the linear problem

$$k'' - T_0 k' + \frac{2(1-N_0)}{(3-N_0)} T_0' k = 1, \tag{4.15a}$$

$$k(0) = 0, \quad k \text{ algebraic as } \quad \hat{\xi} \to \infty, \tag{4.15b,c}$$

where $(\bar{\kappa} - \bar{N})\, k(\hat{\xi}) \equiv \frac{1}{2}(3-N_0)S_1 - T_1' - \frac{1}{2}\bar{N}S_0$. The condition (4.15*c*) allows the solution for k to grow in the form

$$k(\hat{\xi}) \sim K\hat{\xi}^{(2-2N_0)/(3-N_0)} \quad \text{as} \quad \hat{\xi} \to \infty, \tag{4.15d}$$

where the constant K has to be determined from the numerical solution to (4.15*a*–*c*), but the alternative of an exponential growth in k cannot be tolerated. It can be shown from (4.12*a*, *b*) that (4.15*d*) implies

$$\left.\begin{aligned} T_1'(\hat{\xi}) &\sim -K(\bar{\kappa} - \bar{N})\hat{\xi}^{(2-2N_0)/(3-N_0)}, \\ S_1 &\to 0, \end{aligned}\right\} \quad \text{as} \quad \hat{\xi} \to \infty. \tag{4.16}$$

Therefore the outer adjustment zone $Z2$ occurs when $\hat{\xi}$ is $O(\epsilon^{-\gamma})$ [$\gamma = (3-N_0)/(2-2N_0)$], where ϵT_1 overtakes T_0. In $Z2$, effectively, T' is $O(1)$ but $S-1$ is $o(1)$ and the properties are inviscid. Placing $S = 1$ in (4.12*a*, *b*) and neglecting viscous terms, therefore, we have the nonlinear equation

$$-TT'' + T'^2 - 2T' - \tfrac{1}{4}(N_0+1)(N_0-3) = 0 \tag{4.17a}$$

to be satisfied subject to $T(0) = 0$, $T'(0) = \frac{1}{2}(3-N_0)$, $T'(\infty) = \frac{1}{2}(1+N_0)$, from matching with $Z1$ and from (4.12*d*). A regular solution exists only if $T' < \frac{1}{2}(3-N_0)$ [otherwise $T' \to \infty$ as $\hat{\xi} \to \infty$] and it is given implicitly by

$$T = C[\tfrac{1}{2}(3-N_0) - T']^{(3-N_0)/(2-2N_0)}\,[T' - \tfrac{1}{2}(1+N_0)]^{(-1-N_0)/(2-2N_0)}, \quad \text{with} \quad T(0) = 0, \tag{4.17b}$$

where the constant C is unknown but must be positive. We note that, since $N_0 < 1$, the conditions $T' = \frac{1}{2}(3-N_0)$ and $T' = \frac{1}{2}(1+N_0)$ are attainable only for $\bar{\xi} \to 0$ and $\bar{\xi} \to \infty$ respectively ($\bar{\xi} \equiv \epsilon^{\gamma}\hat{\xi}$), which is basically the reason for the existence of zone $Z2$. The merging of $Z2$ (as $\bar{\xi} \to 0$) with $Z1$ (as $\hat{\xi} \to \infty$) is achieved provided

$$\left(\frac{3-N_0}{2C}\right)^{(2-2N_0)/(3-N_0)} (1-N_0)^{(1+N_0)/(3-N_0)} = K(\bar{\kappa} - \bar{N}) \tag{4.18}$$

from (4.13), (4.16), (4.17*b*). Hence the right-hand side of (4.18) must be positive, and so $\bar{\kappa} \lessgtr N$ is permissible depending on whether $K \lessgtr 0$. The numerical solution of (4.15*a*–*c*), to determine the value of K as N_0 varies, is summarized in figures 12 (*a*, *b*)

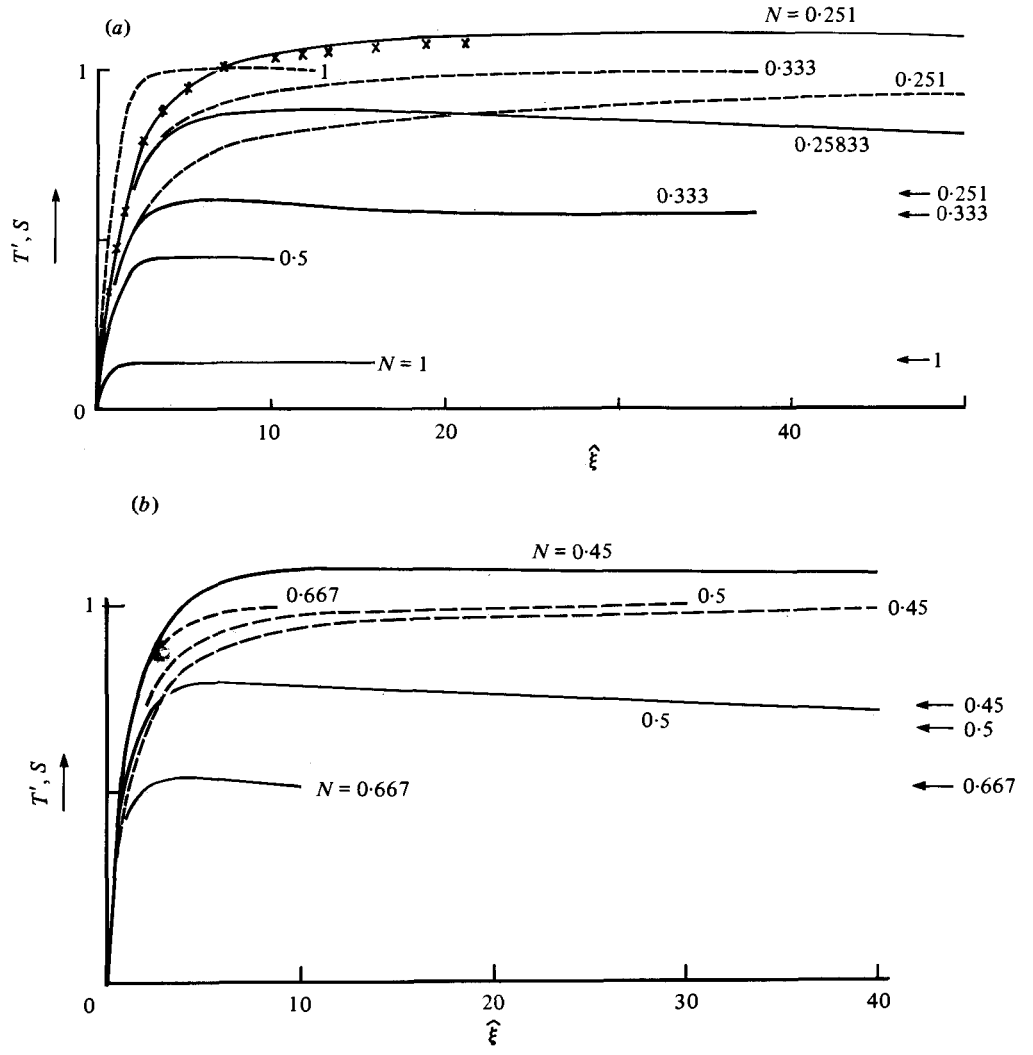

FIGURE 11. For legend see facing page.

(see also appendix). It is found that $K < 0$ if $N_0 > N_{\text{crit}}(= 0{\cdot}1218)$,† $K > 0$ if $N_0 < N_{\text{crit}}$ and $K \propto (N_0 - N_{\text{crit}})^{-1}$ near $N_0 = N_{\text{crit}}$. Hence the suggestion is that if $N > N_{\text{crit}}$ solutions of (4.12*a–d*) exist immediately to the right of the line $\kappa = N(= N_0)$ but not at, or to the left of, $\kappa = N$. A comparison (figure 11*a*) with the full solution of (4.12*a–d*) for $\kappa = 0{\cdot}25$, $N = 0{\cdot}251$ tends to support the singular description proposed in (4.13–18) for $\kappa \to N-$. More significantly for the present work, solutions of (4.12*a–d*) also exist immediately to the left of the line $\kappa = N(= N_0)$ if $N < N_{\text{crit}}$. Hence an advance of the viscous solutions towards the line $\kappa = \kappa_1(N)$ of figure 10 is possible if $N < N_{\text{crit}}$. Finally, to verify firmly that the region of existence of solutions to (4.12*a–d*) does

† N_{crit} is in fact identical with the value $n_0 = 0{\cdot}1217$ of Belcher *et al.* (1972), allowing for numerical error. The reason is that, as $N_0 \to N_{\text{crit}}$, $|k| \to \infty$ (see figure 12*b*) and so effectively k satisfies (4.15*a–c*) but with the constant (1) in (4.15*a*) absent. Hence Belcher *et al.*'s (1972, equation (6.5)) problem is retrieved but with their leading eigenvalue λ having to be zero, which occurs at $N_0 = n_0$.

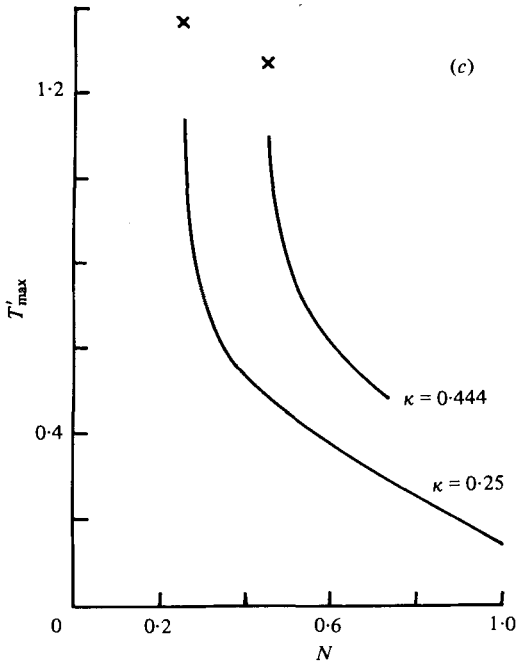

FIGURE 11. Sample numerical solutions of the similarity problem (4.12*a–d*). ——, T'; – – –, S for various values of N. The arrows indicate values of $T'(\infty)$. In (*a*) $\kappa = 0{\cdot}25$, in (*b*) $\kappa = 0{\cdot}444$, and (*c*) shows T'_{max} versus N for those two values of κ. The results are new similarity solutions of the three-dimensional boundary-layer equations. The crosses shown in (*a*) (for T' when $N = 0{\cdot}251$) and in (*c*) (for $\kappa = 0{\cdot}25$, $0{\cdot}444$) follow from the limiting analyses in (4.13)–(4.15), and figure 12 below, near the line $\kappa = N$.

intersect the line $\kappa = \kappa_1(N)$ as required, we note (from the appendix) that, when $N \to 0+$, a perturbation analysis like that of (4.13)–(4.18) can be used to establish the existence of solutions of (4.12*a–d*) just to the left of the line $\kappa = N$ provided only that $N \gg \kappa - N > 0$. Hence the curve $\kappa = \kappa_1(N)$ in (4.10*b*) lies within this region of existence near $N = 0$. Accordingly, viscous solutions exist along $\kappa = \kappa_1(N)$ for a range of values $0 < N < N_{max}$ but not for $N > N_{max}$.

No attempts have been made to determine the value of N_{max} or to solve for the entire zones $A1$, $A2$. Indeed it may be that solutions of a more multistructured kind (cf. Belcher *et al.* 1972) than $A1$–$A2$ exist everywhere along the curve $\kappa = \kappa_1(N)$. Also, order-of-magnitude arguments suggest the presence of further local zones outside $A1$, $A2$, with $\pi - \theta$ of $O(X^{\frac{1}{2}})$. Further comparisons between the proposed singular structure (4.7)–(4.12) for $X \to 0+$ and the full three-dimensional boundary-layer solutions of §§2–3, near the trough line, strongly favour the emergence of the singularity, as §4.3 below shows.

4.2. *The ultimate separated-flow zone* (*B*) *and vortex sheet*

As was stated at the start of § 4, we have suggested that the singular line of § 4.1 sweeps to downstream infinity as $\theta \to \gamma_0+$ (figure 9). In principle the fluid which does not intersect the singular line (see § 5 below for physical interpretation) can flow past that line, on the side $x < x_0(\theta)$, and in particular that flow can continue indefinitely beyond

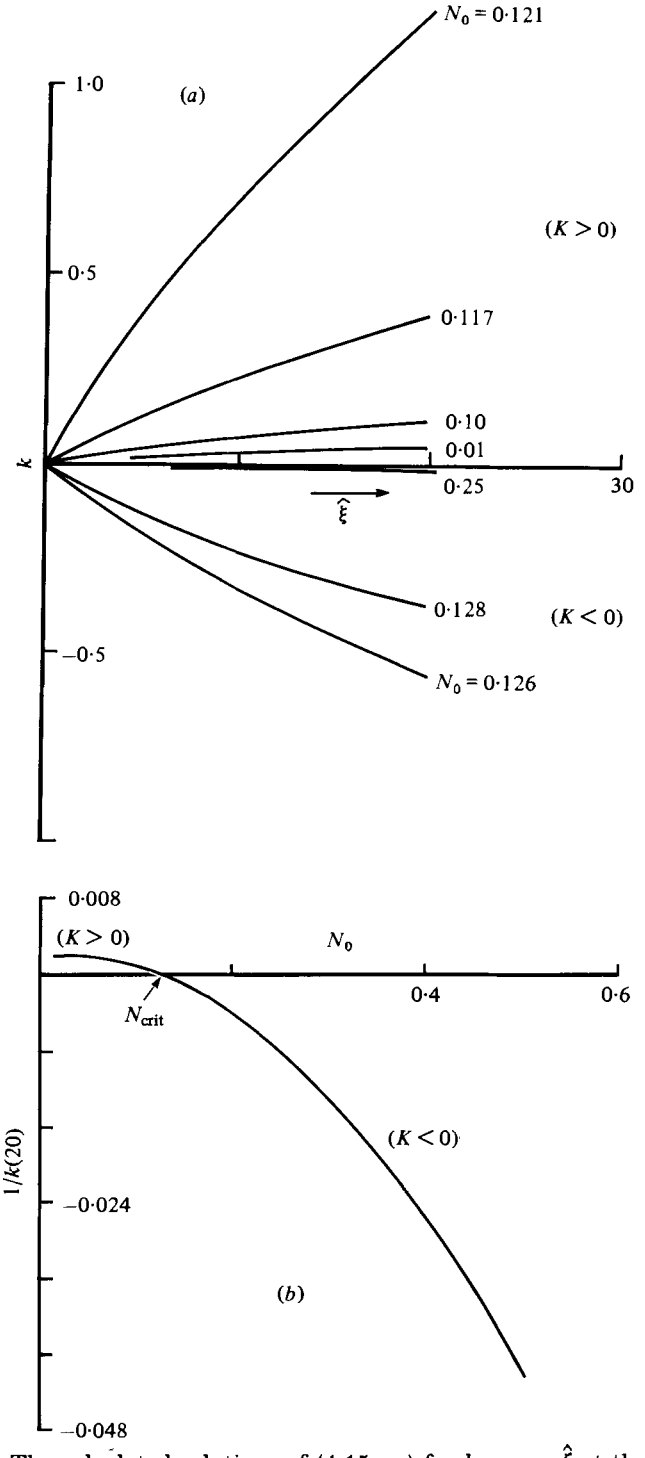

FIGURE 12. (*a*) The calculated solutions of (4.15*a–c*) for k versus $\hat{\xi}$ at the various values of N_0 shown. (*b*) The calculated variation with N_0 of the inverse of k at a typical value (20) of $\hat{\xi}$, shown to illustrate the arguments in (4.15*d*)–(4.18).

the foremost singular point $x = x_0(\pi)$. The boundary condition (2.7) at $\theta = \pi$ is then no longer applicable, of course, and must be replaced by one at the unknown position $x = x_0(\theta) -$ of the singular line, so that some arbitrariness will remain in the following solution for that flow; but the analysis below is concentrated eventually on small values of θ and so is virtually unaffected in character by any change in the boundary conditions from $\theta = \pi$ to $x = x_0(\theta)$. In principle again† part of that flow could remain separated, in the zone B, as we shall show in this subsection. Zone B is the range $0 \leqslant \theta < \Theta_0$, to leading order, where $\Theta_0 \leqslant \gamma_0$ (figure 9). Let us try for a description of the terminal solution in zone B. First, the algebraically singular form of § 4.1 seems out of the question here. For if it did hold then the inviscid equations (4.4a) presumably follow and then, at $\theta = 0$, $\tilde{H}$ would have to vanish in a manner similar to that of (4.7) with θX^{-1} replacing $\bar{\theta}$. But that leads to an axial momentum equation of the type (4.8b) and a contradiction is reached. The contradiction is that $\tilde{P}(0)$ must be positive to preserve the separated flow structure and yet, at the necessary vortex sheet (given by $\eta = \eta_0(0)$ at $\theta = 0$, say), $(\tilde{\mathscr{G}} - N\tilde{\mathscr{F}}\eta_0)$ must vanish to satisfy the conventional inviscid conditions at the sheet. So, at $\eta = \eta_0(0)$, the left- and right-hand sides of (4.8b) have opposite signs. The same contradiction holds at the wall $\eta = 0$ when $\theta = 0$.

We revert, therefore, to an algebraic form in the separated flow zone B and, after some trials, we conclude that a self-consistent account is achievable only if the pressure is asymptotically equal to a positive constant (P_∞, say) throughout zone B. Specifically we propose that, as $x \to \infty$,

$$P \sim P_\infty + o(X^{-1}) \tag{4.19a}$$

(see also (4.22b) below) in B and zone B subdivides into two inviscid regions $B1$, $B3$ and two viscous layers $B2$, $B4$. Here the layer $B2$ is a vortex sheet lying between the outer inviscid region $B1$ and the inner one $B3$, while the layer $B4$ is a reversed sub-boundary layer lying between $B3$ and the wall, as shown in figure 9. The proposition (4.19a) immediately implies the properties

$$D \to D_\infty(\theta), \quad C \sim -xD'_\infty(\theta), \quad E \to D'_\infty(\theta) \quad \text{as} \quad x \to \infty \tag{4.19b}$$

from (2.6b) and from integration with respect to x from $-\infty$ to ∞. Here $D_\infty(\theta)$ is an unknown function of θ, dependent upon the entire flow solution from integration of (2.6b). Then (4.19a, b) suggest the structure $B1$–$B4$ below.

In $B1$, of thickness $O(x^{\frac{1}{2}})$, $\bar{\eta} = Y/x^{\frac{1}{2}}$ is $O(1)$ and

$$(U, V, W) \sim (x^{\frac{1}{2}}\bar{F}(\theta, \bar{\eta}), \quad \bar{G}(\theta, \bar{\eta}), \quad x^{-\frac{1}{2}}\bar{H}(\theta, \bar{\eta})). \tag{4.20}$$

† Following a referee's valuable comments the author wishes to stress the tentative nature of § 4.2. For there is certainly some doubt about the application of this subsection's analysis beyond the foremost singular point $x = x_0(\pi)$ of § 4.1, because of the change in boundary conditions necessary then: see also § 5. On the other hand the author believes the work in § 4.2 to be of importance, both in showing that an understanding of the separation and formation of a genuinely three-dimensional (non-quasi-two-dimensional) vortex sheet from a viscous three-dimensional interaction process is possible, and in providing some further checks on the calculations presented in § 2–3, since it appears (see checks in § 4.3 below) that the relatively short distance between the foremost separation and singular points is still enough for the predicted trends of § 4.2 to emerge satisfactorily in a numerical sense. Despite doubts about the application of § 4.2 to the flow past a relatively large three-dimensional obstruction it is felt that inclusion of § 4.2 is justified, therefore.

Here, from (2.2a–c), $\bar{F}$, $\bar{G}$, $\bar{H}$ satisfy the inviscid equations

$$\left.\begin{aligned} \frac{1}{2}\left(\bar{F}-\bar{\eta}\frac{\partial\bar{F}}{\partial\bar{\eta}}\right)+\frac{\partial\bar{G}}{\partial\bar{\eta}}+\frac{\partial\bar{H}}{\partial\theta} &= 0, \\ \tfrac{1}{2}\bar{F}\left(\bar{F}-\bar{\eta}\frac{\partial\bar{F}}{\partial\bar{\eta}}\right)+\bar{G}\frac{\partial\bar{F}}{\partial\bar{\eta}}+\bar{H}\frac{\partial\bar{F}}{\partial\theta} &= 0, \\ -\tfrac{1}{2}\bar{F}\left(\bar{H}+\bar{\eta}\frac{\partial\bar{H}}{\partial\bar{\eta}}\right)+\bar{G}\frac{\partial\bar{H}}{\partial\bar{\eta}}+\bar{H}\frac{\partial\bar{H}}{\partial\theta} &= 0, \end{aligned}\right\} \tag{4.21a}$$

and the boundary conditions, for $\bar{\eta}\to\infty$,

$$\bar{F}\sim\bar{\eta}-\frac{dD_\infty}{d\theta}\bar{\eta}^{-1}, \quad \bar{G}\to\frac{dD_\infty}{d\theta}, \quad \bar{H}\sim\frac{D_\infty(\theta)}{\bar{\eta}} \tag{4.21b}$$

from (2.6a). The conditions (4.21b) are sufficient to fix the solution in $B1$ (see (4.23)–(4.29) below) but not the position of the vortex sheet $B2$ which forms the lower boundary of $B1$. At $B2$, centred on $\bar{\eta}=\bar{\eta}_0(\theta)$, say (i.e. $Y=x^{\frac{1}{2}}\bar{\eta}_0(\theta)$), the flow in $B1$ must certainly satisfy the stream surface condition (J. H. B. Smith 1975, 1977)

$$\bar{G}=\tfrac{1}{2}\bar{\eta}_0\bar{F}+\bar{H}\,d\bar{\eta}_0/d\theta.$$

But this condition, substituted into (4.21a), leads to the result that $\bar{F}=\bar{G}=\bar{H}=0$ at $\bar{\eta}=\bar{\eta}_0(\theta)$, after integration and applying (2.7) at $\theta=0$. Further inspection (see also (4.23)–(4.29) below) leads to the conclusion that

$$\bar{F}=O[(\bar{\eta}-\bar{\eta}_0(\theta))^{\frac{1}{2}}], \quad \bar{H}=O[(\bar{\eta}-\bar{\eta}_0(\theta))^{\frac{1}{2}}], \quad \bar{G}\sim\tfrac{1}{2}\bar{\eta}_0(\theta)\,\bar{F}+\bar{H}\,d\bar{\eta}_0/d\theta \tag{4.21c}$$

as $\bar{\eta}\to\bar{\eta}_0(\theta)+$ is the constraint fixing the position $\bar{\eta}=\bar{\eta}_0(\theta)$ of the vortex sheet $B2$.

Within the sheet $B2$ (4.21c) assures consistency to leading order and implies that, for viscous forces to be effective, $B2$ has thickness $O(x^{\frac{3}{7}})$. The sheet acts to reduce the velocities from their forms (4.21c) at the upper edge of the sheet to much smaller-sized values at the lower edge. Then, in $B3$, between the sheet and the wall, $\bar{F}$, $\bar{G}$, $\bar{H}$ are identically zero and, instead, the motion there is driven by the need for entrainment into the lower edge of $B2$. The entrainment is due to the (unknown) positive velocity $V=\hat{\kappa}(\theta)x^{-\frac{3}{7}}$ holding at $\bar{\eta}=\bar{\eta}_0(\theta)$ – and implies that in $B3$ (where $0<\bar{\eta}<\bar{\eta}_0(\theta)$)

$$(U,V,W)=(x^{\frac{3}{14}}\bar{\bar{F}}(\bar{\eta},\theta),x^{-\frac{3}{7}}\bar{\bar{G}}(\bar{\eta},\theta),x^{-\frac{11}{14}}\bar{\bar{H}}(\bar{\eta},\theta)). \tag{4.22a}$$

It is also necessary for consistency that the azimuthal pressure gradient and inertial forces should balance in $B3$. Hence

$$P\sim P_\infty-x^{-\frac{11}{7}}\bar{\bar{P}}(\theta) \tag{4.22b}$$

and, from (4.22a, b) and (2.2a–c), $\bar{\bar{F}},\bar{\bar{G}},\bar{\bar{H}},\bar{\bar{P}}$ satisfy the inviscid equations

$$\left.\begin{aligned} \left(\tfrac{9}{14}\bar{\bar{F}}-\tfrac{1}{2}\bar{\eta}\frac{\partial\bar{\bar{F}}}{\partial\bar{\eta}}\right)+\frac{\partial\bar{\bar{G}}}{\partial\bar{\eta}}+\frac{\partial\bar{\bar{H}}}{\partial\theta} &= 0, \\ \bar{\bar{F}}\left(\tfrac{9}{14}\bar{\bar{F}}-\tfrac{1}{2}\bar{\eta}\frac{\partial\bar{\bar{F}}}{\partial\bar{\eta}}\right)+\bar{\bar{G}}\frac{\partial\bar{\bar{F}}}{\partial\bar{\eta}}+\bar{\bar{H}}\frac{\partial\bar{\bar{F}}}{\partial\theta} &= 0, \\ \bar{\bar{F}}\left(-\tfrac{11}{14}\bar{\bar{H}}-\tfrac{1}{2}\bar{\eta}\frac{\partial\bar{\bar{H}}}{\partial\bar{\eta}}\right)+\bar{\bar{G}}\frac{\partial\bar{\bar{H}}}{\partial\bar{\eta}}+\bar{\bar{H}}\frac{\partial\bar{\bar{H}}}{\partial\theta} &= \frac{d\bar{\bar{P}}}{d\theta}. \end{aligned}\right\} \tag{4.22c}$$

The boundary conditions in $B3$ impose tangential flow as the wall is approached and matching with $B2$ at $\bar{\eta} = \bar{\eta}_0(\theta) -$, in the form

$$\bar{\bar{G}} \to 0 \quad \text{as} \quad \bar{\eta} \to 0+, \quad \bar{\bar{G}} \to \hat{\kappa}(\theta) \quad \text{as} \quad \bar{\eta} \to \bar{\eta}_0(\theta) - . \tag{4.22d}$$

Lastly, region $B4$ is required to reduce the slip velocities $\bar{\bar{F}}(0,\theta), \bar{\bar{H}}(0,\theta)$ resulting from (4.22c–d) to zero at the wall.

End conditions are again required, at $\theta = 0$ and $\theta = \Theta_0$, for all regions $B1$–$B4$.

While complete solutions for $B1$–B4 for $0 \leqslant \theta < \Theta_0$ have not been attempted, nevertheless some encouraging features do emerge from a study of the properties of $B1$–$B4$ near the peak line $\theta = 0$. There we expect that, for $\theta \to 0$ in $B1$,

$$(\bar{F}, \bar{G}, \bar{H}) \sim (f(\bar{\eta}) + \theta^2 f_1(\bar{\eta}),\, g(\bar{\eta}) + \theta^2 g_1(\bar{\eta}),\, \theta\bar{h}(\bar{\eta}) + \theta^3 \bar{h}_1(\bar{\eta})), \tag{4.23a}$$

$$D_\infty(\theta) \sim \theta D_1 + \theta^3 D_3 \tag{4.23b}$$

because of (2.7); here the unknown constants D_1 and D_3 are expected to be positive and negative respectively. From (4.21a,b), therefore, $\bar{f}, \bar{g}, \bar{h}$ must satisfy the problem

$$\left.\begin{aligned} \frac{1}{2}\left(\bar{f} - \bar{\eta}\frac{d\bar{f}}{d\bar{\eta}}\right) + \frac{d\bar{g}}{d\bar{\eta}} + \bar{h} &= 0, \\ \tfrac{1}{2}\bar{f}\left(\bar{f} - \bar{\eta}\frac{d\bar{f}}{d\bar{\eta}}\right) + \bar{g}\frac{d\bar{f}}{d\bar{\eta}} &= 0, \\ -\tfrac{1}{2}\bar{f}\left(\bar{h} + \bar{\eta}\frac{d\bar{h}}{d\bar{\eta}}\right) + \bar{g}\frac{d\bar{h}}{d\bar{\eta}} + \bar{h}^2 &= 0, \end{aligned}\right\} \tag{4.24a}$$

$$\bar{f} \sim \bar{\eta} - \frac{D_1}{\bar{\eta}}, \quad \bar{h} \sim \frac{D_1}{\bar{\eta}}, \quad \bar{g} \to D_1 \quad \text{as} \quad \bar{\eta} \to \infty. \tag{4.24b}$$

As in §4.1 the nonlinear inviscid problem can be solved in an implicit form. The equations in (4.24a) are manipulated to yield an ordinary differential equation for $\bar{f}(\bar{\eta})$ above. Then, in the latter equation, $d\bar{f}/d\bar{\eta}$ is treated as a function of $\bar{f}$. Integration and application of (4.24b) then yields the (implicit) solution

$$\bar{f} - D_1^{\frac{1}{2}} \tan^{-1}(D_1^{-\frac{1}{2}}\bar{f}) = \bar{\eta} - \tfrac{1}{2}\pi D_1^{\frac{1}{2}} \tag{4.25a}$$

for $\bar{f}(\bar{\eta})$ (with $-\frac{1}{2}\pi < \tan^{-1} < \frac{1}{2}\pi$). It follows that, from (4.21c),

$$\bar{\eta}_0(0) = \tfrac{1}{2}\pi D_1^{\frac{1}{2}} \tag{4.25b}$$

determines the vortex sheet position at $\theta = 0$, and that

$$\bar{f} \sim [3D_1(\bar{\eta} - \bar{\eta}_0(0))]^{\frac{1}{3}} \quad \text{as} \quad \bar{\eta} \to \bar{\eta}_0(0)+. \tag{4.25c}$$

Similar behaviour as $\bar{\eta} \to \bar{\eta}_0(0)+$ occurs in $\bar{g}, \bar{h}$ since, from (4.24a), (4.25a),

$$\bar{h} = \frac{D_1\bar{f}}{D_1 + \bar{f}^2}, \quad \bar{g} = \tfrac{1}{2}\bar{\eta}\bar{f} - \frac{\bar{f}^4}{2(D_1 + \bar{f}^2)}. \tag{4.25d}$$

Hence the occurrence of the one-third powers of $(\bar{\eta}-\bar{\eta}_0)$ referred to just below (4.21*c*) is demonstrated. However, to reinforce the demonstration an examination of the next-order terms in (4.23*a*, *b*) is necessary and also proves fruitful in regard to the comparisons in §4.3 below. From (4.21*a*, *b*) the problem

$$\left.\begin{aligned} \frac{1}{2}\left(f_1-\bar{\eta}\frac{d\bar{f}_1}{d\bar{\eta}}\right)+\frac{d\bar{g}_1}{d\bar{\eta}}+3\bar{h}_1 &= 0,\\ \bar{f}\bar{f}_1-\tfrac{1}{2}\bar{\eta}\frac{d}{d\bar{\eta}}(\bar{f}\bar{f}_1)+\bar{g}\frac{d\bar{f}_1}{d\bar{\eta}}+\bar{g}_1\frac{d\bar{f}}{d\bar{\eta}}+2\bar{h}\bar{f}_1 &= 0,\\ -\frac{1}{2}\left(\bar{f}\bar{h}_1+\bar{f}_1\bar{h}+\bar{\eta}\bar{f}\frac{d\bar{h}_1}{d\bar{\eta}}+\bar{\eta}\bar{f}_1\frac{d\bar{h}}{d\bar{\eta}}\right)+\bar{g}\frac{d\bar{h}_1}{d\bar{\eta}}+\bar{g}_1\frac{d\bar{h}}{d\bar{\eta}}+4\bar{h}\bar{h}_1 &= 0, \end{aligned}\right\} \tag{4.26a}$$

$$\bar{f}_1\sim\frac{-3D_3}{\bar{\eta}},\quad \bar{h}_1\sim\frac{D_3}{\bar{\eta}},\quad \bar{g}_1\to 3D_3\quad\text{as}\quad\bar{\eta}\to\infty \tag{4.26b}$$

governs $\bar{f}_1,\bar{g}_1,\bar{h}_1$. After manipulating (4.26*a*) to derive an equation for f_1 alone involving $\bar{f}$, $\bar{g}$, $\bar{h}$, $\bar{\eta}$, we treat $\bar{f}_1$ as a function of $\bar{f}$ and, using (4.25*a*, *d*), we obtain the ordinary differential equation

$$\begin{aligned} &\frac{\bar{f}^3}{12}\frac{d^3\bar{f}_1}{d\bar{f}^3}+\frac{\bar{f}^2}{(D_1+\bar{f}^2)}\left(\frac{\bar{f}^2}{4}-\frac{7D_1}{12}\right)\frac{d^2\bar{f}_1}{d\bar{f}^2}+\frac{2D_1\bar{f}}{(D_1+\bar{f}^2)^2}\left(\frac{D_1}{12}-\frac{\bar{f}^2}{4}\right)\frac{d\bar{f}_1}{d\bar{f}}\\ &\qquad+\frac{1}{6(D_1+\bar{f}^2)^3}(3D_1\bar{f}^4+30D_1^2\bar{f}^2+35D_1^3)\bar{f}_1=0 \end{aligned} \tag{4.27a}$$

for $\bar{f}_1(\bar{f})$. One solution of (4.27*a*) is readily found to be $\bar{f}_1=(\bar{f}^2+D_1)\bar{f}^{-2}$ and on substituting $\bar{f}_1=(\bar{f}^2+D_1)f^{-2}\chi$ we arrive at an associated Legendre equation for $d\chi/d\bar{f}$. Its solution satisfying (4.26*b*) is

$$\frac{d\chi}{df_C}=A_C(1-\xi^2)^4(33\xi^5-30\xi^3+5\xi), \tag{4.27b}$$

where $\xi(2f_C^2+1)=1, \bar{f}=D_1^{\frac{1}{2}}f_C$ and A_C is an unknown constant. Hence the solution for $\bar{f}_1$ satisfying (4.26*b*) is

$$\bar{f}_1=-\left(\frac{\bar{f}^2+D_1}{2^{\frac{3}{2}}\bar{f}^2}\right)A_C\int_0^{\xi}(1-\xi_1^2)^{\frac{7}{2}}(33\xi_1^7-30\xi_1^3+5\xi_1^{-\frac{1}{2}})\,d\xi_1. \tag{4.27c}$$

Here $A_C=6D_3/5D_1^{\frac{1}{2}}$. The solutions for $\bar{h}_1,\bar{g}_1$ then follow from (4.26*a*). In particular (4.27*c*) shows that as $\bar{\eta}\to\bar{\eta}_0(0)+$

$$\bar{f}_1\sim\lambda_1(\bar{\eta}-\bar{\eta}_0(0))^{-\frac{3}{2}}, \tag{4.27d}$$

where $\lambda_1=1{\cdot}721A_C\,D_1/(3D_1)^{\frac{3}{2}}$. At first sight (4.27*d*) seems to contradict the one-third power law proposed just below (4.21*c*), but further inspection establishes that (4.27*d*) merely acts as a displacement of the leading-order term's behaviour (4.25*c*). For, in the implied new layer defined by $\bar{\eta}-\bar{\eta}_0(0)=O(\theta^2)$, wherein the terms $\theta^2\bar{f}_1$ and $\bar{f}$ of (4.23*a*) become comparable (according to (4.25*c*), (4.27*d*)), the solution for $\bar{F}$ is simply a displacement of (4.25*c*), to leading order:

$$\bar{F}=\theta^{\frac{3}{2}}\left[\frac{\bar{\eta}-\bar{\eta}_0(0)}{\theta^2}+\frac{3\lambda_1}{(3D_1)^{\frac{1}{2}}}\right]^{\frac{1}{3}}(3D_1)^{\frac{1}{3}}+O(\theta^{\frac{4}{3}}). \tag{4.28}$$

Hence (4.21*c*) implies that, for $\theta \ll 1$, the vortex sheet position is described by

$$\bar{\eta}_0(\theta) \sim \tfrac{1}{2}\pi D_1^{\frac{1}{2}} + 2{\cdot}064 D_3 D_1^{-\frac{1}{2}}\theta^2 + O(\theta^4) \tag{4.29}$$

and (4.28) confirms the one-third power law at the vortex sheet. Since $D_3 < 0$ (4.29) yields a physically sensible shape for the vortex sheet locally near the peak line.

Further terms in (4.23*a*) may be obtained in principle, and similar local analyses near the peak line may be made for regions *B*2–*B*4. In *B*3, for instance, under the assumption that

$$(\bar{\bar{F}}, \bar{\bar{G}}, \bar{\bar{H}}) \sim (\bar{\bar{F}}_0, \bar{\bar{G}}_0, \theta\bar{\bar{H}}_0) \quad \text{as} \quad \theta \to 0+ \tag{4.30}$$

in (4.22*c*), the equations for $\bar{\bar{F}}_0, \bar{\bar{G}}_0, \bar{\bar{H}}_0$ may be manipulated into one equation for $(d\bar{\bar{F}}_0/d\bar{\eta})$ as a function of $\bar{\bar{F}}$. Then the substitutions $d\bar{\bar{F}}_0/d\bar{\eta} = z^{\frac{5}{9}}\phi(z)$, $\bar{\bar{F}}_0 z = -1$, lead to Bessel's equation for $\phi(z)$. The relevant solution for $\phi(z)$ is proportional to $K_{\frac{10}{9}}(z)$, the $\frac{10}{9}$-order Bessel function of imaginary argument, and integration with respect to $\bar{\bar{F}}_0$ yields $\bar{\bar{F}}_0(\bar{\eta})$. The required boundary conditions $\bar{\bar{G}}_0(0) = (0)$, $\bar{\bar{G}}_0(\bar{\eta}_0(0)) = \kappa(0)$ (from (4.22*d*)) are readily satisfied and the reversed flow property, that $\bar{\bar{F}}_0(\bar{\eta}) < 0$ for $0 < \bar{\eta} \leqslant \bar{\eta}_0(0)$, is obtained.

4.3. *Comparisons with the full solutions*

First, an alternative presentation of the full three-dimensional solutions of §3 for τ, τ_θ, P (case 1) is given in figure 13 to underline the progress with respect to x of the θ variation of the flowfield. The singular, and strongly attached, nature of the flow near the trough line according to §4.1 then seems to be in keeping with the full solutions of figure 13, as does the less dramatic behaviour proposed in §4.2 near the peak line. In particular, with the estimated values $N = 0{\cdot}17$, $\kappa = 0{\cdot}194$, $P_0 = 2{\cdot}22$, $x_0(\pi) = 6{\cdot}4$ suggested for case 1 (see also figures 10 and 14), the asymptotes of (4.2), (4.7) which are also shown in figure 13 produce fairly good agreement with the full solution near the trough line, at the last two x stations shown. Next, a plot (against x) of the values of $P/P', \tau/\tau'$ (prime $\equiv d/dx$) and P along the trough line (case 1, figure 2), given in figure 14, also lends some support to the proposed existence of a singularity at a finite value $(x_0(\pi))$ of x, with the above values of N, κ, $x_0(\pi)$, P_0; note, incidentally, that far upstream the asymptotes $P/P' \to 1$, $\tau/\tau' \to \infty$ (exponentially) of (2.5) are reproduced in figure 14. The very fact that, in contrast with figure 14, an exponential or algebraic behaviour of P as $x \to \infty$ along the trough line would yield P/P' tending to a constant or to infinity, respectively, downstream also adds weight to the belief in a singular form ((4.2), which for P/P' is linear as $x \to x_0(\pi) -$). Further agreement in a qualitative sense is derived by comparing the velocity profiles U, W near the trough line according to §4.1 (figure 10) with the full solutions of figure 7.

Finally, comparisons between §4.2 and the results of §3 along and near the peak line are drawn in figure 15. Figure 15(*a*) presents comparisons of the velocity profiles from case 2 (figure 7) with those of §4.2, where x is measured from the separation point and the representative value $D_1 = 2$ is taken; the agreement is not discouraging, especially in view of the limited downstream range covered numerically in §§2–3. We note also that in figure 2 the pressure gradient along the peak line reaches a maximum just before the end of the integration there, so that an approach to (4.19*a*) far downstream is not inconsistent. Figure 15(*b*) gives comparisons of the curves on which

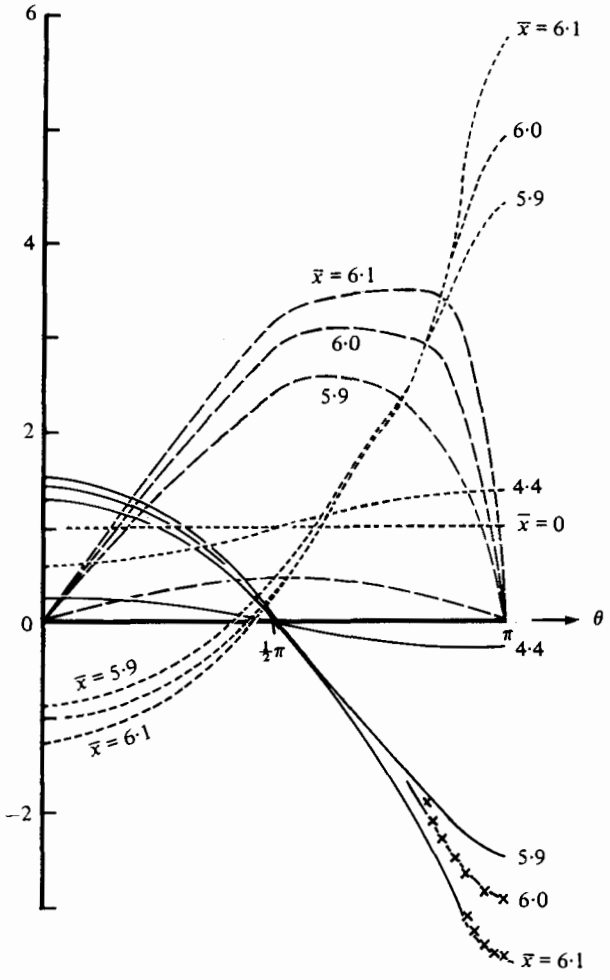

FIGURE 13. The calculated variation with θ of the axial skin friction τ, the pressure P, the azimuthal skin friction τ_θ, at various values of $\bar{x}$ ($= x - x_{-\infty}$), for case 1 of §3. ——, P; – – –, τ_θ; ·····, τ. The crosses indicate the predictions of §4.1 (see (4.2), (4.7)) for P at $\bar{x} = 6{\cdot}0$, $6{\cdot}1$.

$U = 0$ from §3 (figure 8) with the vortex sheet curve of §4.2 (see (4.29)). We remark that D_1 in (4.29) is replaced by $\partial D\,(x, 0)/\partial\theta$ in figure 15(*b*), since these two values are equivalent as $x \to \infty$ anyway (according to (4.23*b*)) while the replacement seems to compensate for the limited extent of the downstream integration range, and improved agreement is thereby obtained. In fact, with the estimated value $D_3 = -0{\cdot}5$ suggested by the variation of $D(x, \theta)$ in figure 5(*b*), the development of the numerical solutions of §§2–3 is remarkably close (figure 15*b*) to the asymptotic prediction (4.29) even for such small values of x.

5. Implications and further discussion

By no means, of course, can it be claimed yet that a full account (for all values of θ) of the terminal structure of the upstream flow response (free interaction) studied numerically in §§2–3 has been advanced. Indeed, the mechanism of the terminal

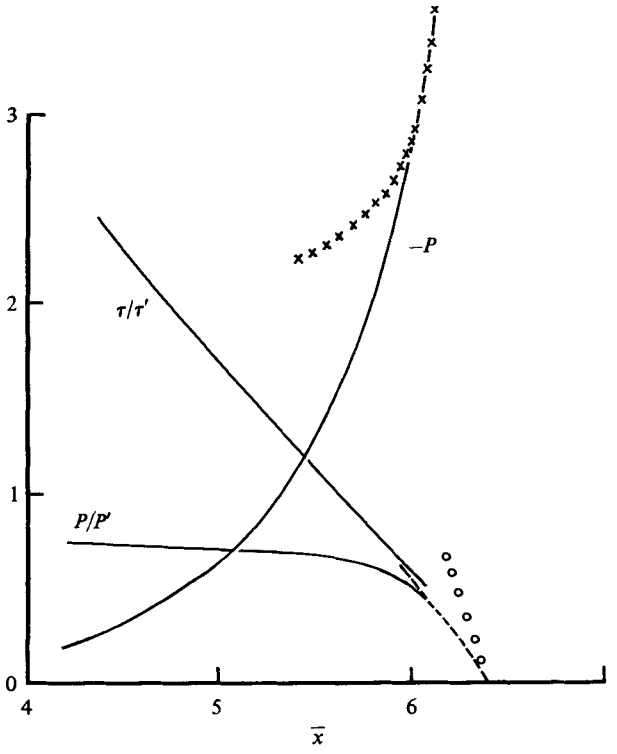

FIGURE 14. Comparison, along $\theta = \pi$, of the full numerical solutions (for case 1) for $P, P/P', \tau/\tau'$ (from § 3) with the local terminal predictions (from § 4.1). The former are shown by solid curves, the latter by, respectively, crossed, dashed and open-circle curves. Also, note that $P/P' \to 1$ upstream, in line with the starting form (2.5).

singularity near the trough line (§ 4.1) alone is such a delicate matter that any hope of a full account, for all values of θ, seems very remote. Nevertheless, it is felt that the comparisons in § 4.3, between the proposed terminal forms and the full solutions near the trough and peak lines, do add considerable weight to the arguments of §§ 4.1, 4.2; further, the very existence of a singularity arising in the upstream flow response is enough in itself to enable some important inferences to be drawn (see below) in the context of flow past three-dimensional obstacles which are steeper than the three-dimensional boundary layer examined in this paper. So, despite the undeniably large amount of work that would be required to verify a full account for all values of θ and the analytical difficulties inherent in treating three-dimensional boundary-layer flows, we believe that the analyses in § 4 do provide a consistent starting point for such a complete description, if necessary, of the terminal structure of the upstream free interaction. We believe further that a singular termination of the increasingly attached part of the flowfield, as in § 4.1, is inevitable for any nontrivial upstream response, no matter how the upstream response starts in (2.5). Certainly all the starting forms tested numerically by the author led to strong attachment phenomena akin to those described in § 3. To provide support for any asymptotic proposals describing the complete terminal structure (figure 9), however, presumably the considerable task of numerically

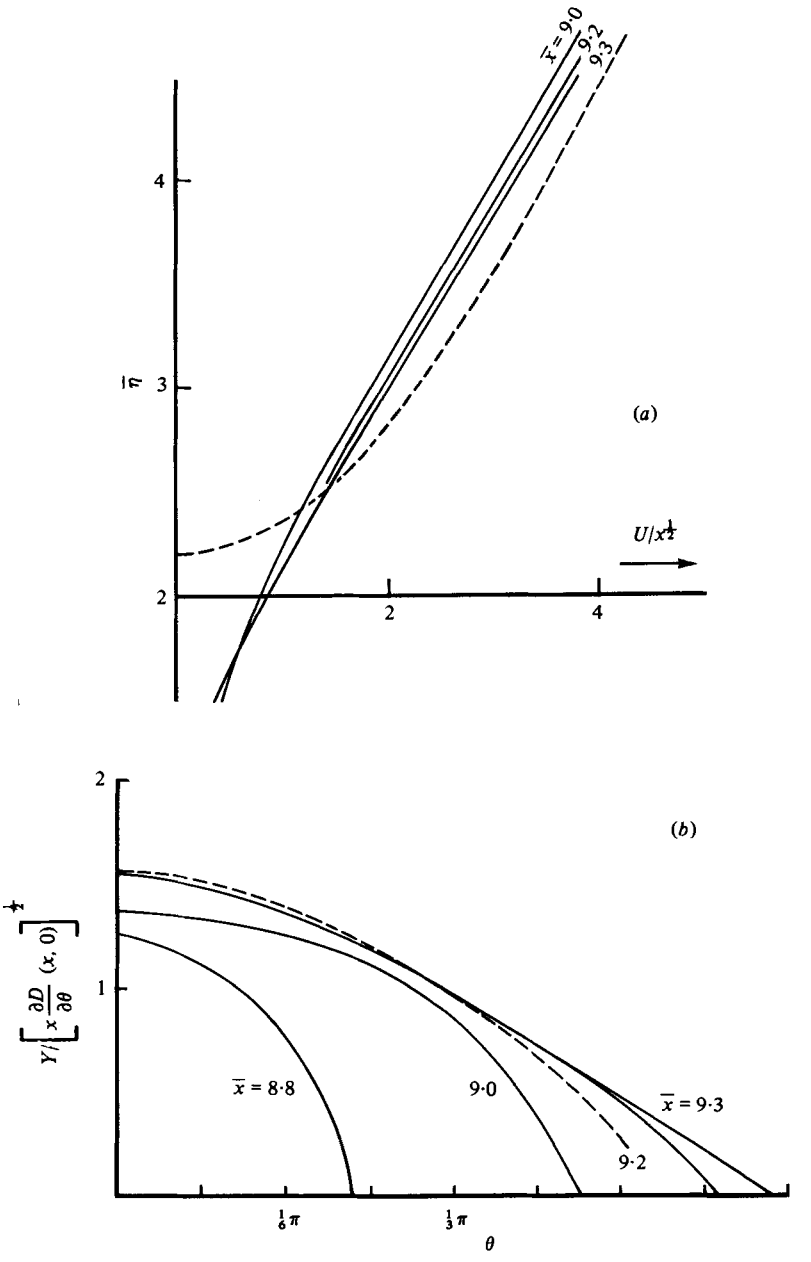

FIGURE 15. (*a*) Comparison between theory (§4.2) and calculations (§3) of velocity profiles, in the form $x^{-\frac{1}{4}}U$ versus $x^{-\frac{1}{4}}Y$, around the separated flow region. The solid curves are the full numerical solutions from §3; the dashed curve is the predicted asymptote from (4.25*a*). (*b*) Comparison between theory (§4.2) and calculations (§3) of the curves of zero streamwise velocity ($U = 0$) in the cross-flow (Y,θ) plane, for the various values of $\bar{x} = x - x_{-\infty}$ shown; the solid curves are as in (*a*), while the dashed curve gives the prediction (4.29).

continuing the free interaction of §§ 2–3 beyond the foremost singular point ($x = x_0(\pi)$), towards the whole singular curve $x = x_0(\theta)$ ($\pi \geqslant \theta > \gamma_0$), would have to be faced. The question of matching the attached part of the flowfield (§ 4.1) to the separated part (§ 4.2) would also represent a considerable analytic and numerical challenge.

Before discussing the broader implications of the free interaction studied in this paper, we wish to draw attention to a number of points of further interest. It is worth while emphasizing first the genuinely three-dimensional nature of the entire free interaction above. If the flow remained two-dimensional there would be no upstream response at all, because of the zero displacement condition (2.3*c*), as the starting forms (2.5) show. The terminal forms of §§ 4.1, 4.2 likewise reflect the necessity of three-dimensionality in the motion, without which the solutions of § 4 could not exist. By contrast, if the displacement is nonzero, as in the three-dimensional triple-deck problems of Smith *et al.* (1977) and Professor O. R. Burggraf & Dr P. W. Duck (1978–9, private communications) (see also the comments on pipe flows below), then the terminal forms of the free interaction in both the attached and separated parts of the flowfield can still be two-dimensional phenomena even when the flow upstream develops in a three-dimensional fashion. This would suggest further that three-dimensional free interactions with nonzero displacement may yield singular similarity solutions throughout a wide range of the κ, N plane of figure 10, if a line of symmetry (corresponding to our line $\theta = \pi$) is present. In fact, with zero or nonzero displacement, it is possible that a three-dimensional free interaction may lead to a wide range of line- or point-singularities apart from the new similarity forms studied in § 4.1. Since the three-dimensional boundary-layer equations are involved many of the nonlinear phenomena of rotating fluids, for example, are accessible in principle as local terminal forms, including the subtleties of the Belcher *et al.* (1972) ladder structure as well as the simpler forms of Rott & Lewellen (1966) and Greenspan (1968). Again, the emergence of a vortex sheet downstream in the separated flow of § 4.2 raises the possibility of such complex phenomena as vortex spirals, associated with the flow past moderately sized obstacles, developing as an asymptotic part of a three-dimensional free interaction. Whether or not such singularities or vortex formations can arise in three-dimensional free interaction studies remains the subject of further research.

We consider finally the direct implications of the upstream flow response studied in §§ 2–4 for three-dimensional pipe flows and external flows. In both cases the occurrence of the singularity (§ 4.1) in the strongly attached motion is of paramount importance, of course. First, for pipe flows, if a particular bounded obstacle defined by

$$r = 1 - hR^{-\frac{1}{3}}f(x, \theta)$$

[$Y = hf(x, \theta)$ in I with $f(x, \theta)$, an $O(1)$ function of x, θ, being zero outside a bounded domain of the x, θ plane] were present at the pipe wall, then for h of $O(1)$ the motion upstream of the obstacle would be described by only part of the free interaction of §§ 2–3. As h increases, however, presumably the upstream response must increase and when $h \gg 1$ (but $h \ll R^q$ for all $q > 0$, to retain the flow structure of § 2) the flow variables immediately upstream of the onset of the obstacle must be asymptotically large in order to accommodate the asymptotically large change in boundary conditions at the obstacle. Hence when $h \gg 1$ the obstacle must start in the neighbourhood of, and just upstream of, the foremost singular point $x = x_0(\pi)$. As h increases, therefore, the upstream response cannot be pushed infinitely far upstream: it remains confined to

$O(1)$ distances ahead of the obstacle and, as $h \to \infty$, the flow variables (U, V, W, P) remain $O(1)$ at such distances upstream. The unbounded increase necessary in the flow variables is concentrated immediately ahead of the obstacle (i.e. for $x_0(\pi) - x \ll 1$) and thereafter, not upstream. These properties are similar to the singularity properties of certain two-dimensional free interaction flows (Stewartson 1971; Smith 1977*b*) [despite the fact that here the separated flow region (§ 4.2) could in principle continue to infinity downstream] and they lead to an explanation of the flow features for obstacles which are steeper than those (of slope $R^{-\frac{1}{8}}$) above. For the effect of the concentration of relatively large pressures, in particular, around the obstacle and beyond as h increases becomes spread out in the inviscid core flow II of § 2 and, most significantly, the core flow response ahead of the obstacle increases indefinitely (in contrast with the upstream response of the boundary layer I above) as h increases indefinitely. Eventually, therefore, the core flow perturbation response, originally of order $R^{-\frac{3}{8}}$ in (2.4*a*), will grow to become comparable to the boundary-layer response and the slip velocity associated with the core flow perturbation will interact with the original Poiseuille flow near the wall. Hence we envisage that, as the obstacle increases in severity, the next stage of upstream (and overall) flow response, different from that of §§ 2–4 (and Sykes 1979), will arise when the core flow displacement produced by the obstacle itself is sufficient to introduce a nonzero displacement effect at the edge of the boundary layer I instead of the zero displacement of (2.3*c*). Furthermore, the boundary layer will then still be confined to $O(1)$ distances ahead of the obstacle.

A similar, although less clear, interpretation is readily available for external flows, granted the limitations set by the periodicity condition used here (see § 1). Bearing in mind that, for external flows, the obstacle for which §§ 2–4 describes the upstream flow response is small compared with the triple-deck size (Smith *et al.* 1977), we may infer that as the obstacle increases in severity the next stage of upstream response distinct from that of §§ 2–4 will occur when the obstacle is sufficiently large to produce a nonlinear response of the triple-deck interaction kind or equivalent, with the displacement then being nonzero. Both in three-dimensional pipe flows and external flows, therefore, the advance from the present zero-displacement structure to the (unknown) structure of the flow upstream of a truly severe obstruction, of dimensions of order one, appears to be via a structure involving a nonzero displacement, of the triple-deck (Stewartson 1974; Smith *et al.* 1977) or of the core-feedback (Smith 1978*b*) type.

The author wishes to thank Dr R. I. Sykes for his interest in the present work, Professor S. C. R. Dennis and Dr D. B. Ingham for their comments on (2.7) and the referees for their valuable comments. The financial support of the Natural Science and Engineering Research Council of Canada and the hospitality of the Applied Mathematics Department at U.W.O., during a large part of this research, are gratefully acknowledged, as is the receipt of a Commonwealth Travel Bursary from the Royal Society.

Appendix. The solutions of (4.12*a–d*) and (4.15*a–c*) near $N = \kappa = 0$ and $N = \kappa = 1$

Local analyses of (4.12*a–d*), (4.15*a–c*) near $N = \kappa = 0, 1$ are required for (*inter alia*) the purpose of checking on the numerical work and conclusions of § 4.1. Consider first

the solution of (4.15*a–c*) when $N_0 \to 0+$. The Falkner–Skan problem (4.14*a*, *b*) for T_0, which we transform to

$$\tilde{T}''' - \tilde{T}\tilde{T}'' + \beta(1 - \tilde{T}'^2) = 0, \tag{A 1}$$

$$\tilde{T}(0) = \tilde{T}'(0) = 0, \quad \tilde{T}'(\infty) = 1, \tag{A 2}$$

to match the notation of Jones & Watson (1963) (here

$$T_0 = [\tfrac{1}{2}(3 - N_0)]^{\frac{1}{2}}\tilde{T}(\tilde{\xi}), \quad \tilde{\xi} = [\tfrac{1}{2}(3 - N_0)]^{-\frac{1}{2}}\tilde{\xi}, \quad \beta = 2N_0/(3 - N_0)),$$

then splits into two sublayers $F1$, $F2$ of thickness $O(\beta^{-\frac{1}{2}})$, $O(\beta^{-\frac{1}{2}}e^{1/\beta})$ respectively ($\beta \ll 1$). In $F1$, $\tilde{T} = \beta^{\frac{1}{2}}\tilde{T}_1 + \ldots$ with $\tilde{\xi} = \beta^{-\frac{1}{2}}\xi_1$ and so from (A 1)

$$\tilde{T}_1''' - \tilde{T}_1\tilde{T}_1'' + 1 = 0. \tag{A 3}$$

The boundary conditions on (A 3) are $\tilde{T}_1(0) = \tilde{T}_1'(0) = 0$ (from (A 2)) but the outer constraint in (A 2) is unattainable in $F1$. Instead we impose

$$\tilde{T}_1 \sim \xi_1(2\ln\xi_1)^{\frac{1}{2}} \quad \text{as} \quad \xi_1 \to \infty. \tag{A 4}$$

Then in the outer layer $F2$, where $\tilde{\xi} = \beta^{-\frac{1}{2}}e^{\xi_2/\beta}$, $\tilde{T} = \tilde{\xi}\tilde{T}_2 + \ldots$ and from (A 1)

$$-\tilde{T}_2\tilde{T}_2' + 1 - \tilde{T}_2^2 = 0. \tag{A 5}$$

Here the solution must satisfy the outer constraint in (A 2), i.e. $\tilde{T}_2 \to 1$ as $\xi_2 \to \infty$, and match with (A 4) as $\xi_2 \to 0$. The solution of (A 5) is therefore

$$\tilde{T}_2 = (1 - e^{-2\xi_2})^{\frac{1}{2}}. \tag{A 6}$$

Similarly, the problem (4.15*a–c*) for $k(\tilde{\xi})$ must also split into two as $N_0, \beta \to 0$, where k now satisfies

$$\frac{d^2k}{d\tilde{\xi}^2} - \tilde{T}\frac{dk}{d\tilde{\xi}} + \tfrac{2}{3}(1-\beta)\,k\tilde{T}' = \tfrac{1}{3}(2+\beta). \tag{A 7}$$

In $F1$, $k = \beta^{-\frac{1}{2}}k_1 + \ldots$, implying that from (A 7)

$$k_1'' - \tilde{T}_1 k_1' + \tfrac{2}{3}k_1\tilde{T}_1' = \tfrac{2}{3} \tag{A 8}$$

and

$$k_1(0) = 0, \quad \xi_1^{-\frac{2}{3}}k_1 \text{ logarithmic as } \xi_1 \to \infty, \tag{A 9}$$

from (4.15*b*) and analysing (A 8) for $\xi_1 \gg 1$. Once (A 8), (A 9) are solved the development through sublayer $F2$ to the condition (4.15*c*) may be ensured as in (A 5), (A 6) for $\tilde{T}$. The solutions of (A 3), (A 4) for $\tilde{T}_1$ and (A 8), (A 9) for k_1 have been found numerically, are shown in figure 16, and have the properties $\tilde{T}_1''(0) = 1{\cdot}436$, $k_1'(0) = 5{\cdot}025$. The implied asymptote $\tilde{T}''(0) \sim 1{\cdot}436\beta^{\frac{1}{2}}$ for $\beta \to 0+$ agrees satisfactorily with the Falkner–Skan solutions of (A 1), (A 2) when β is small, while the implied asymptote

$$\frac{dk}{d\tilde{\xi}}(0) \sim 6{\cdot}801N_0^{-\frac{1}{2}} \quad \text{for} \quad N_0 \to 0+ \tag{A 10}$$

agrees satisfactorily with the full solutions of (4.15*a–c*) for small N_0, as figure 17 shows. Further, the solutions confirm that the property $K > 0$ (see figure 12*a*, *b*) persists as $N_0 \to 0+$.

Second, the problem (4.15*a–c*) is also analysable when $N_0 \to 1$. Suppose $N_0 = 1 - \delta$ (where $\delta \ll 1$). Then, to leading order, T_0 satisfies $T_0''' - T_0T_0'' + 1 - T_0'^2 = 0$ with (4.14*b*),

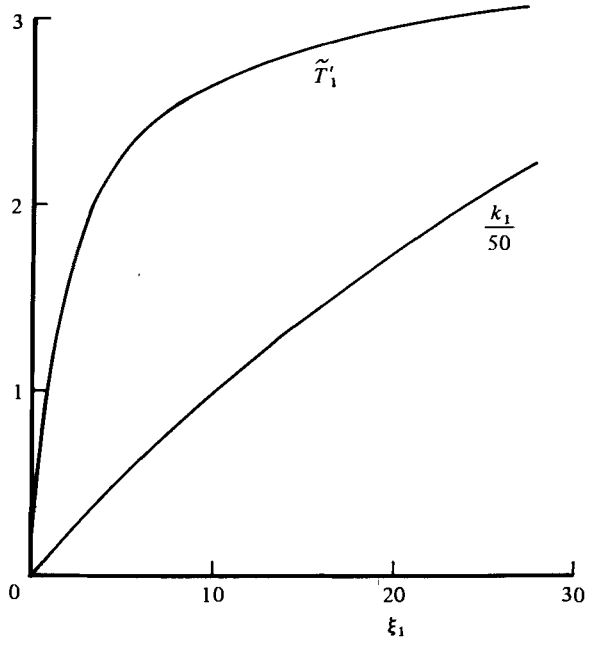

FIGURE 16. The numerical solutions of (A 3), (A 4) and (A 8), (A 9) for $\tilde{T}'_1$ and k_1 *versus* ξ_1.

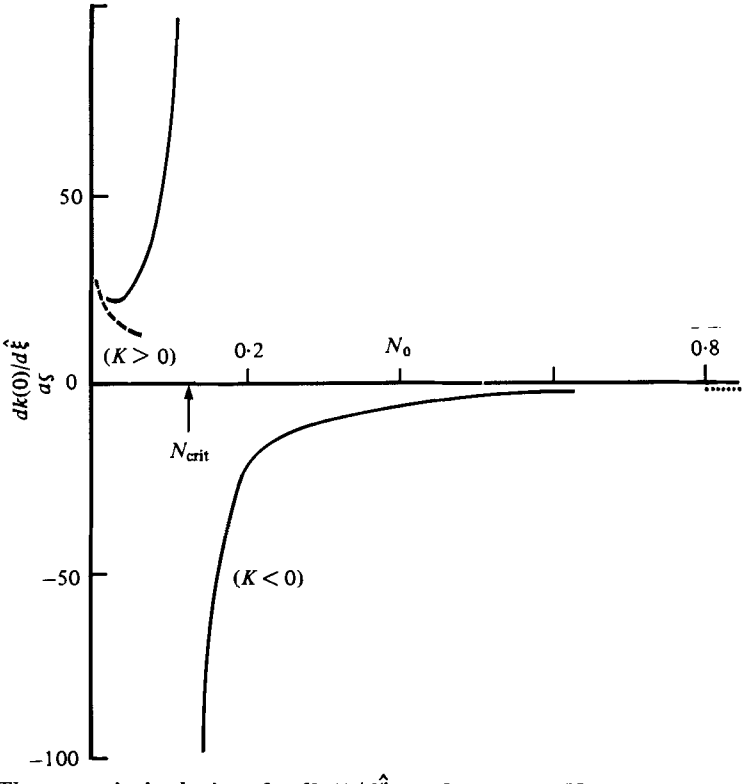

FIGURE 17. The numerical solutions for $dk(0)/d\hat{\xi}$ as a function of N_0 from (4.15*a–c*) (solid curves), compared with the limits (A 10) near $N_0 = 0$ (dashed curve) and (A 14) near $N = 1$ (dotted line).

the solution of which is obtainable analytically after a double integration (Jones & Watson 1963), while k satisfies $k''-T_0k'=1$ when $\hat{\xi}$ is $O(1)$. Hence

$$k=\int_0^{\hat{\xi}}\exp\left(\int_0^{z_1}T_0(z)\,dz\right)\int_\infty^{z_1}\exp\left(-\int_0^{z_2}T_0(z_3)\,dz_3\right)dz_2\,dz_1 \tag{A 11}$$

and $k\sim-\ln\hat{\xi}$ as $\hat{\xi}\to\infty$. Again, therefore, an outer adjustment layer is called for to satisfy (4.15*c*, *d*), and this occurs where $\hat{\xi}=\exp(\xi_3/\delta)$ with ξ_3 of $O(1)$. There

$$k=\delta^{-1}k_3+\ldots,\quad T_0=\hat{\xi}+\ldots\quad\text{and so}\quad -k_3'+k_3=1.$$

The merging (as $\xi_3\to0$) with (A 11) (as $\hat{\xi}\to\infty$) and the outer constraint (4.15*c*) or (4.15*d*) are satisfied by the solution

$$k_3=1-e^{\xi_3} \tag{A 12}$$

since (A 12) yields

$$k\sim-\delta^{-1}\hat{\xi}^\delta\quad\text{for}\quad\hat{\xi}\to\infty \tag{A 13}$$

in line with (4.15*d*). It follows that $K\sim-(1-N_0)^{-1}$ is negative as $N_0\to1-$, confirming further the conclusions of §4.1 concerning K. Also, (A 11) yields the asymptote

$$\frac{dk}{d\hat{\xi}}(0)\to-1{\cdot}4\quad\text{as}\quad N_0\to1-, \tag{A 14}$$

which agrees satisfactorily with the numerical solutions of (4.15*a*–*c*) (figure 17).

Third, we may use and extend the work of (A 1)–(A 9) to examine the solutions of the full problem (4.12*a*–*d*) near $N=\kappa=0\,(=\beta)$. In particular, one important suggestion from (A 3), (A 8) is that, since in $F1$ $T_0'\sim\beta^{\frac{1}{2}}$ whereas the $O(\epsilon)$ perturbations T_1', S_1 (of (4.13)) $\sim\beta^{-\frac{1}{2}}$, the expansion of (4.13) will remain valid in principle as $N_0\to0+$ provided $\epsilon\ll N_0$. Assuming that, as $N\to0$, $\kappa\sim N+\epsilon$ when $\epsilon\ll N$, we may then split the solution of (4.12*a*–*d*) into two layers $F1$, $F2$. However, the ensuing analysis essentially reproduces that of (4.13)–(4.18) and (A 1)–(A 10), and so it is readily found that the suggestion above is justified. Hence solutions exist in particular along the line $\kappa=\kappa_1(N)$ of figure 10(*a*) for $N\ll1$, since $\kappa_1\sim N+N^2$ there from (4.10*b*). Fourth, and similarly, the work of (A 11)–(A 14) may be extended to allow examination of the solutions of (4.12*a*–*d*) near $N=\kappa=1$. Once again, however, the resultant analysis follows much the same pattern as above, i.e. (A 11)–(A 14). The details need not be pursued here, but they do confirm that solutions of (4.12*a*–*d*) exist only to the right of the line $\kappa=N$ as $N\to1-$, in keeping with §4.1.

REFERENCES

Belcher, R. J., Burggraf, O. R. & Stewartson, K. 1972 *J. Fluid Mech.* **52**, 753.

Dennis, S. C. R., & Chang, G. Z. 1970 *J. Fluid Mech.* **42**, 471.

Goldstein, S. 1948 *Quart. J. Mech. Appl. Math.* **1**, 43.

Greenspan, H. P. 1968 *The Theory of Rotating Fluids.* Cambridge University Press.

Hobson, E. W. 1931 *Theory of Spherical and Ellipsoidal Harmonics.* Cambridge University Press.

Jones, C. W. & Watson, E. J. 1963 *Laminar Boundary Layers* (ed. L. Rosenhead), cha. V. Oxford University Press.

Messiter, A. F. 1975 *AGARD Conf. Proc.* 168 *on Flow Separation, May* 1975, paper no. 4.

Messiter, A. F. 1979 *Proc. 8th U.S. Nat. Cong. of Appl. Mech., June* 1978, *Los Angeles* (in the press).

REYHNER, T. A. & FLÜGGE-LOTZ, I. 1968 *Int. J. Nonlinear Mech.* **3**, 173.
RIZZETTA, D. P., BURGGRAF, O. R. & JENSON, R. 1978 *J. Fluid Mech.* **89**, 535.
ROTT, N. & LEWELLEN, W. S. 1966 *Prog. Aero. Sci.* **7**, 111.
SMITH, F. T. 1973 *J. Fluid Mech.* **57**, 803.
SMITH, F. T. 1974 *J. Inst. Math. Applic.* **13**, 127.
SMITH, F. T. 1976*a* *Quart. J. Mech. Appl. Math.* **29**, 343.
SMITH, F. T. 1976*b* *Mathematika* **23**, 62.
SMITH, F. T. 1977*a* *Proc. Roy. Soc.* A **356**, 443.
SMITH, F. T. 1977*b* *J. Fluid Mech.* **79**, 631.
SMITH, F. T. 1978*a* *R.A.E. Tech. Rep.* TR78095.
SMITH, F. T. 1978*b* *J. Inst. Math. Applic.* **21**, 145.
SMITH, F. T. 1979*a* *J. Fluid Mech.* **92**, 171.
SMITH, F. T. 1979*b* *J. Fluid Mech.* **90**, 725.
SMITH, F. T. & STEWARTSON, K. 1973*a* *Proc. Roy. Soc.* A **332**, 1.
SMITH, F. T. & STEWARTSON, K. 1973*b* *J. Fluid Mech.* **58**, 143.
SMITH, F. T. & DUCK, P. W. 1977 *Quart. J. Mech. Appl. Math.* **30**, 143.
SMITH, F. T., SYKES, R. I. & BRIGHTON, P. W. M. 1977 *J. Fluid Mech.* **83**, 163.
SMITH, J. H. B. 1975 *AGARD Conf. Proc.* 168 *on flow separation*, paper 31; also *R.A.E. Tech. Memo. Aero.* 1620.
SMITH, J. H. B. 1977 *R.A.E. Tech. Rep.* TR77-58.
STEWARTSON, K. 1970 *Proc. Roy. Soc.* A **319**, 289.
STEWARTSON, K. 1971 *Quart. J. Mech. Appl. Math.* **24**, 387.
STEWARTSON, K. 1974 *Adv. Appl. Mech.* **14**, 145.
STEWARTSON, K. & WILLIAMS, P. G. 1969 *Proc. Roy. Soc.* A **312**, 181.
STEWARTSON, K. & WILLIAMS, P. G. 1973 *Mathematika* **20**, 98.
SYCHEV, V. V. 1972 *Izv. Akad. Nauk S.S.S.R. Mekh, Zhidk. Gaza* **3**, 47.
SYKES, R. I. 1979 Submitted to *Proc. Roy. Soc.* A.
WILLIAMS, P. G. 1975 *Proc. 4th Int. Conf. Numerical Methods in Fluid Dynamics, Boulder* 1974. Springer.